U.PORTO
FACULDADE DE CIÊNCIAS
UNIVERSIDADE DO PORTO

The role of ADP-ribosylation factor-like 15 in influenza A virus infection

Ana Rita Henriques Ramos do Nascimento

Dissertação de Mestrado apresentada à
Faculdade de Ciências da Universidade do Porto em
Biologia Celular e Molecular

2015

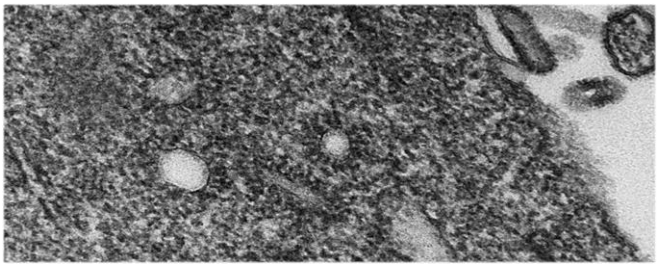

The role of ADP-ribosylation factor-like 15 in influenza A virus infection

Ana Rita Henriques Ramos do Nascimento

Mestrado em Biologia Celular e Molecular

Departamento de Biologia
2015

Orientador
Maria João Amorim, PhD

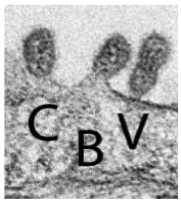

INSTITUTO GULBENKIAN DE CIÊNCIA

U.PORTO

FACULDADE DE CIÊNCIAS
UNIVERSIDADE DO PORTO

Todas as correções determinadas pelo júri, e só essas, foram efetuadas.

O Presidente do Júri,

Porto, _____/_____/_____

Dedicated to my parents Anabela and José António

Acknowledgements

I would like to start by thanking my advisor, Maria João, for all her kindness and support. One can only be so lucky in finding someone so passionate about what they do, particularly when one does research. Your support started long before my enrollment in this Master's program, when I was a young student fascinated by viruses. In few months, your constant enthusiasm became contagious, in a wonderful way. During this past year, you were also vital in encouraging me when the scenery was not as bright, helping me realize that we are lucky individuals simply because we are able to answer our own questions through our research. Thank you for your guidance, dedication, and wise words throughout this time.

I also would like to address dear Marta and Silvia for their support and valuable advice in challenging experiments, and also Bárbara, Zoe and Megan for their day-to-day help at the lab that was truly appreciated. Overall, the smallest things can sometimes be overlooked or unappreciated, yet I am candidly thankful for them all.

Then, I express my gratitude to my parents, sister, and our wonderful family. Even without a scientific background, you always taught us to think critically, yet humorously, about all subjects. Without you, I would not have gotten this far.

Finally, my friends also had an important part in accompanying me in the course of this thesis. I want to thank all of you, those from *the North*, the ones that are far away and those from home. You had the difficult burden of bearing with my quirky disposition, and always embracing my nerdy perspectives on life.

Contents

List of Tables and Figures

Abbreviations

A549	Alveolar 549 cells
ARF	ADP-ribosylation factor
ARL	ARF-like
BSA	Bovine serum albumin
CA	Constitutively active
DN	Dominant negative
GAP	GTPase activating protein
GAPDH	Glyceraldehyde 3-phosphate dehydrogenase protein
GBF1	Golgi Brefeldin-A resistant guanine nucleotide exchange Factor 1
GEF	Guanine exchange factor
H or HA	Hemagglutinin
HEK 293T	Human embryonic kidney cells 293T
IAV	Influenza A virus
M1	Matrix protein 1
M2	Matrix protein 2
MDCK	Madin-Darby canine kidney cells
MOI	Multiplicity of infection
N or NA	Neuraminidase
NEP	Nuclear export protein
NP	Nucleoprotein
p.i.	Post-infection
PA	Polymerase acidic protein
PB1	Polymerase basic subunit 1
PB2	Polymerase basic subunit 2
PFU	Plaque forming unit
RdRp	RNA-dependent RNA polymerase
TGN	Trans Golgi network
UTR	Untranslated region
vRNA	Viral RNA
vRNP	Viral ribonucleoprotein
WT	Wild-type

Resumo

O vírus influenza A é o agente causador de epidemias e pandemias de gripe, com forte impacto na população. O estudo do ciclo de replicação do vírus, e das vias celulares que utiliza, constitui uma resposta às limitações associadas à vacinação ou prescrição de drogas antivirais.

O genoma deste vírus é constituído por 8 segmentos (vRNPs), que são replicados no núcleo da célula hospedeira e exportados para o citoplasma onde se dá a montagem do virião e saída para o espaço extracelular. Para a montagem, todos os componentes necessitam de chegar a locais específicos da célula. O *recycling endosome* é um compartimento usado pelo vírus para o transporte de vRNPs para estes locais na membrana plasmática. No entanto, apenas a proteína celular Rab11 foi identificada como reguladora deste processo. Para além das Rab, o transporte vesicular também é regulado pela família *ADP-ribosylation factors* (ARF). Um rastreio de 26 membros da família de proteínas ARF foi realizado em células infectadas com o vírus influenza A e revelou um candidato, ARF-like 15 (ARL15), objecto de estudo desta tese.

Os resultados obtidos demonstram que a ARL15 influencia positivamente a infecção, visto que a sua depleção reduziu em dez vezes os títulos virais, efeito revertido após expressão exógena da proteína. Adicionalmente, a localização intracelular da ARL15 mostrou-se sensível à infecção com influenza A, com translocação da proteína do cis-Golgi para um compartimento não-identificado nas fases iniciais da infecção. Ensaios de silenciamento resultaram na acumulação citoplasmática de vesiculas com vRNP, sugerindo que a proteína ARL15 tem uma função no transporte de vRNPs para os locais de montagem do viriao. Mais ainda, o nosso trabalho sugere que a ARL15 pode contribuir para a inactivação da Rab11 visto afectar negativamente a ligação dos vRNP à Rab. A inactivação da Rab11 é um novo passo necessário para a formação do complexo genómico que contém os 8 segmentos. A formação deste complexo está na origem de estirpes que causam pandemias. A identificação de novos mecanismos entre o hospedeiro e o vírus no que toca à montagem do virião é importante para a implementação de estratégias antivirais.

Palavras-chave: Vírus influenza A, família ARF, proteínas ARL, trafego de vRNPs, montagem do virião.

Abstract

Influenza A virus (IAV) is the infectious agent that causes epidemic and pandemic events of flu, which have high impact in the human population. The study of the viral lifecycle, and the cellular pathways that it highjacks, presents an alternative avenue for treatment of IAV infection, as current vaccines and antiviral treatments present many drawbacks.

The virus has an eight-part segmented RNA genome in the form of ribonucleoproteins (vRNPs) which are replicated in the nucleus of the host cell but must be exported to the cytoplasm for viral assembly, budding and release. Assembly comprises convergence of all virion components to specific sites in the cell. vRNPs use the recycling endosome for transport to the assembly sites at the plasma membrane. Only one host protein, Rab11, has been defined to participate in this process. In addition to Rab proteins, vesicular transport is also regulated by the family of ADP-ribosylation factors (ARF). A preliminary screen involving 26 members of the ARF-family in IAV infected cells resulted in the identification of a promising candidate protein, ARL15, which for this reason is the object of study in this thesis.

We demonstrate that ARL15 positively impacts IAV infection as its depletion leads to a 10 fold reduction in virus production, which was reverted by overexpressing ARL15. Furthermore, ARL15's intracellular localization was sensitive to infection, by translocating from the cis-Golgi to an unidentified compartment, at the early stages of infection. The depletion of ARL15 resulted in the accumulation of vRNP-carrying vesicles in the cytoplasm, suggesting that ARL15 plays a role in transporting vRNPs to sites of virion assembly. Additionally, we present indirect evidence that ARL15 might contribute to a step in infection subsequent to vRNP ligation to Rab11 vesicles and we propose that it might promote Rab11 inactivation. This is a novel step in infection of IAV involved in the formation of the 8-segment genome core. Assembly of the genome core is the basis of reassortment that leads to the emergence of pandemic strains and therefore, unraveling key host-pathogen mechanisms underlying viral assembly will certainly contribute to implement novel antiviral strategies.

Keywords: influenza A virus, IAV, ADP-ribosylation factor-like, ARL, ARF-family, vRNP trafficking, IAV assembly.

CHAPTER 1 | Introduction

1.1. Influenza – Impact and Disease

Influenza viruses are the infectious agents responsible for a contagious acute respiratory disease, commonly referred to as flu[1], an important disease in humans. It causes yearly epidemics with associated high mortality and economic burden, and occasional pandemics of devastating consequences. For these reasons, circulating influenza viruses in humans are continuously surveilled, as the basis for vaccine production to mitigate dramatic outcomes of the infection. There are three types of influenza viruses: A, B and C, all associated with human disease and provoking different levels of severity[2].

Influenza A viruses (IAV), the most relevant of the three types to human health, are found in various animals including humans, pigs, bats, horses, and wild birds, the latter being the primary reservoir for most subtypes of influenza A viruses[3]. The vast diversity among IAV has led to the establishment of categories based on the viral antigens, i. e. the two main proteins at the surface of the virus: hemagglutinin (H or HA) and neuraminidase (N or NA). There are 18 different hemagglutinin and 11 neuraminidase subtypes[4,5] (H1 to H18 and N1 to N11 respectively that are shown in table 1.1).

This diversity, in part, originates from the viral optimization to the biology of each host it infects to increase its fitness. The viral fine-tuning to each biological system results in the restriction of viral growth to species sharing similar processes. However, on rare occasions, IA viruses are able to jump the species barrier, infecting other hosts[5]. These events have had serious impact in human health, provoking disease of variable outcomes. Table 1.2 summarizes IAV outbreaks of different origins that occurred in humans during recent history with variable severity. These outbreaks include sporadic incursions of viruses, such as the avian strains H5N1[6] and H7N9[7], that resulted in high mortality rates in infected people but were unable to become established in the human population. These infections did not spread, but had a global effect in creating awareness to potential pandemics. The table also includes viruses that provoked generalized disease, such as the well-known Spanish Flu that killed over 40 million people worldwide[8]. In this particular

case, the virus was able to successfully establish in the human population and to be perpetuated, causing annual episodes of influenza infections that are normally known as epidemic or seasonal influenza.

Table 1.1. Diversity in subtypes of viral surface proteins HA and NA, with host distribution. Adapted from[4]

Hemagglutinin					Neuraminidase				
Subtype	**People**	**Poultry**	**Pigs**	**Bats/ other**	**Subtype**	**People**	**Poultry**	**Pigs**	**Bats/ other**
H1	●	●	●		**N1**	●	●	●	
H2	●	●	●		**N2**	●	●	●	
H3	●	●	●	other animals	**N3**		●		
H4		●	●	other animals	**N4**		●		
H5	●	●	●		**N5**		●		
H6	●	●			**N6**	●	●		
H7	●	●		other animals	**N7**	●	●		other animals
H8		●			**N8**	●	●		other animals
H9	●	●	●		**N9**	●	●		
H10	●	●			**N10**				bats
H11		●			**N11**				bats
H12		●							
H13		●							
H14		●							
H15		●							
H16		●							
H17				bats					
H18				bats					

The establishment in a new host requires adaptation to a different biological environment[3]. To accomplish these adaptations, the virus uses many strategies, taking advantage of the nature of its genome, which is RNA of negative polarity, and composed of eight different segments that work as independent entities[2]. The virus has high mutation rates, on account of the error prone RNA polymerase that it encodes[39]. This results in constant mutations that reshape viral antigens (antigenic drift) and allow continued infections in the same host. Second, in addition to mutagenesis, the segmented nature of the virus allows genome mixing upon co-infection of the same cell, a process called reassortment. Reassortment greatly augments viral diversity and evolution and may produce antigenic shifts (substitution) in the combination of HA-NA subtypes present in the surface of the virion[10]. Such complex events are for example behind the pandemics of

1957, 1968 and 2009 (Table 1.2, below). In both cases, host species jump or viral reassortment, strains unknown to the immune system may emerge with unpredictable consequences to human health.

Table 1.2. Human IAV outbreaks in recent history.

Year	Subtype	Name	Event	Origin	Statistics	Ref
1889-92	H2N2(?)	Russian Flu	Pandemic	(?)	1 million deaths worldwide.	8
1918-57	H1N1	Spanish Flu	Pandemic	Avian	40 to 50 million deaths worldwide.	8
1957-68	H2N2	Asian Flu	Pandemic	Avian, human	1 to 2 million deaths worldwide.	8
1968-69	H3N2	Hong Kong Flu	Pandemic	Avian, human	1-3 million infected, 700 000 deaths worldwide.	8
1969-Present	H3N2	-	Seasonal	-	40 000 deaths per year (overall seasonal data).	11,12
1977-2009	H1N1	Russian Flu epidemic	Epidemic then Seasonal	Reintroduced strain	Epidemic caused 70 000 deaths in the USA.	8
1999	H9N2	-	New strain	Avian	Illness in 2 children in Hong Kong. Zero deaths.	13
2003	H7N7	-	New strain	Avian	83 confirmed cases in Netherlands, zero deaths.	14
2003-Present	H5N1	-	New strain with pandemic potential	Avian	700 infections, 400 deaths.	6
2004	H7N3	-	New strain	Avian	2 infected zero deaths in Canada.	15
2009-10	H1N1	Swine/ Mexican Flu	Pandemic	Avian, human, swine	Over 18 000 deaths worldwide.	16
2010-Present	H1N1	-	Seasonal	-	40 000 deaths per year (overall seasonal data).	11,12
2013-Present	H7N9	-	New strain with pandemic potential	Avian	571 laboratory-confirmed cases, 212 deaths in China.	7

Epidemic strains currently circulating in humans include the H1N1 and H3N2[12]. These strains have become established in humans after the pandemic events of 2009 and 1968, respectively. Mutations lead to the selection of strains with modified epitopes of HA or NA[10]. Immune defenses developed against the viral proteins HA and NA were no longer able to recognize the new antigens, and thus would not protect the infected individual[17]. According to the World Health Organization and the European Center for Disease Prevention and Control (ECDC), every year approximately 100 million people are affected by IAV in Europe, Japan and the USA, and nearly 40 thousand people die prematurely in the European Union alone[11]. The infectious period usually lasts a week, with patients

presenting sore throats, body aches and fatigue. Even though most individuals recover without requiring medical treatment, people suffering from diabetes, asthma, heart disease, cancer, pregnant women, children, the elderly and immunocompromised individuals are considered risk groups. In these cases, infection can lead to severe medical complications, such as pneumonia, and even result in death[1].

In order to mitigate the effects of influenza infection, a yearly vaccination program has been implemented worldwide. Surveillance provides data on circulating strains and predicts the ones that are most likely to become prevalent in the following year[18]. Vaccines are updated once the reactivity of produced antibodies to circulating strains diminishes[17]. This expensive updating system requires constant investigation and surveillance as it is based on predictive methods that are not devoid of error. Last year, vaccines designed for the northern hemisphere failed to include a H3N2 strain that became prevalent during the flu season, reaching 70% of H3N2 cases of infection[19]. Figure 1.1a illustrates the switch in the prevalent subtype from H1N1 to H3N2 by analyzing circulating viruses in humans over the years of 2013-2015. During this period, the vaccine composition was not updated, with the trivalent vaccine including the following strains: H1N1 (A/California/7/2009 pandemic-like virus), H3N2 (A/Texas/50/2012-like virus) and influenza B (B/Massachusets/2/2012-like virus)[20]. The analysis of patient's samples by the Center for Disease Control (CDC, USA) concluded that individuals were producing antibodies that reacted against an antigenically and genetically distinct strain of influenza A H3N2 to that in circulation. This new variant had suffered an antigenic drift escaping the immune response developed to the H3N2 strain included in the vaccine. Figure 1.1b highlights the reshaping of the viral protein HA, the most abundant of the viral proteins at the surface of the virus. The prevalence of H3 subtype, over that of H1, was a novel epidemiological mark and greatly increased the effect of H3 inefficient vaccines. This vaccine was updated for administration to the southern hemisphere to include the strain H3N2 A/Switzerland/9715293/2013 which showed to be effective in preventing viral infection.

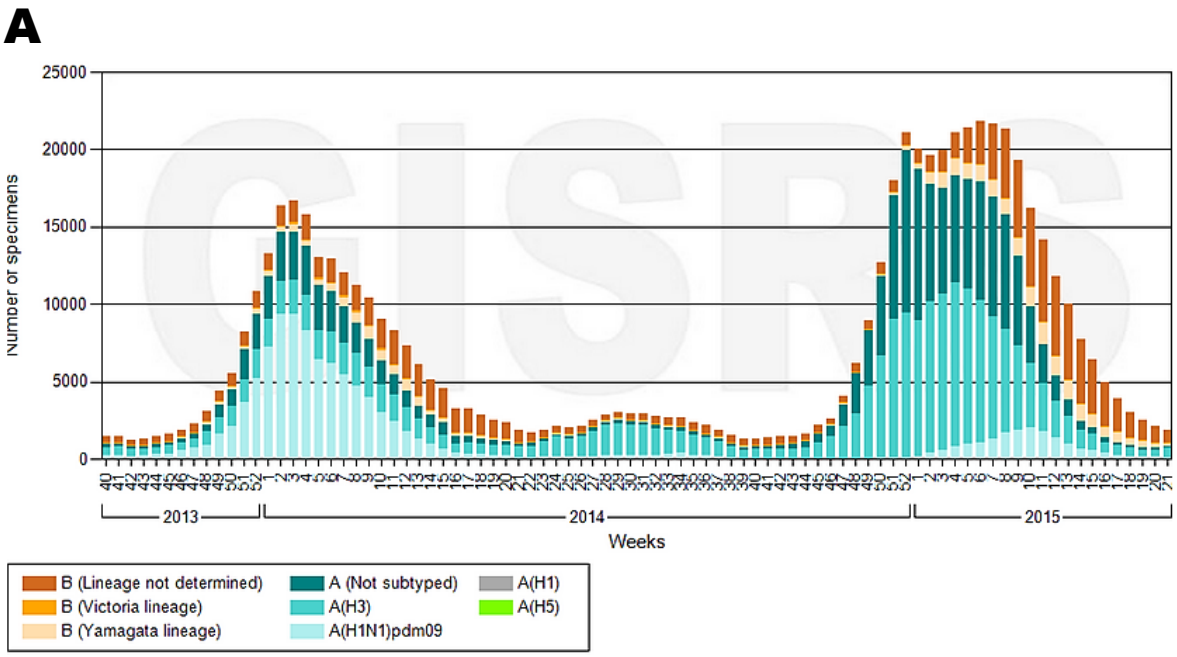

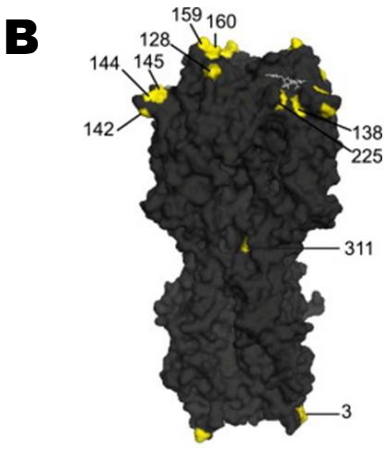

Figure 1.1. Emerging new H3N2 strain during 2014-15 winter season. a) Number and subtypes of influenza specimens circulating worldwide during winter season 2013-14 and 2014-15[21]**. b)** Changes in epitopes of HA between the H3N2 A/Texas/50/2012 vaccine strain and most viruses isolated during the 2014–2015 Northern Hemisphere influenza season. Altered residues: L3I, T128A, A138S, R142G, N144S, N145S, F159Y or F159S, K160T, N225D, Q311H[22].

In 2015, the CDC issued a statement informing the general population of the inefficacy of the vaccine due to the widespread dissemination of the mutated H3N2 strain[23]. Medical staff were instructed to pay special attention to patients presenting flu-like symptoms, and to directly prescribe antiviral medication. Antivirals currently available are inhibitors of viral protein neuraminidase function, thus preventing viral release. The drugs would reduce symptoms, shorten the length of illness, keep patients out of hospitals and prevent further spread of the virus. Supported by the current situation with antibiotics, the widespread prescription of antivirals to symptomatic patients generated controversy, based on the possibility of emergence of more aggressive and resistant strains in the population[24]. In accordance, drugs administered in the past that targeted viral entry are no

longer effective in combating circulating strains[24]. The low numbers of effective antivirals to overcome influenza infections has led to an increase in research to identify novel therapeutical strategies.

Influenza B viruses also contribute to the burden of seasonal epidemics. However, contrary to IAV, antigenic differences in influenza B are limited as illustrated by the two lineages that circulate since the 1980s: Victoria and Yamagata[25]. Mutagenesis rate in antigenic proteins is lower in influenza B, and thus antigenic drift was suggested to have a much less significant role in flu epidemics[3]. The host range of influenza B is restricted to humans and seals[26]. Despite the limited number of susceptible hosts, it has been shown that influenza B is capable of undergoing genome mixing by reassortment, but the significance of these phenomena in epidemics is yet to be understood[27]. Although significant, the number of cases of influenza B in humans is inferior to those provoked by influenza A (figure 1.1a), but still justifies its inclusion in vaccines[12]. The symptoms of influenza B are less severe than those attributed to IAV and the lack of an animal reservoir and differences with IAV prevents severe outbreaks and pandemics in humans. Consequently, influenza B constitutes a smaller problem for human health[27].

Influenza C viruses cause only mild infections in humans and pigs, and are associated with infrequent cases of localized outbreaks[28]. The impact of these infections is very low, and this type is not considered during vaccine design[3].

Overall, IAV is a major human pathogen with severe impact in human population. In spite of tight surveillance, yearly updated vaccination and extensive antiviral drug development incentives, the virus continues to provoke epidemics and occasional pandemics with severe outcomes. Therefore, novel strategies to target IAV infection are required, whose identification greatly depends on the thorough knowledge of IAV lifecycle and the characteristics of the virion.

1.2. Influenza A – Virion

The influenza A virus represented in figure 1.2a belongs to the *Orthomyxoviridae* family. It has a viral envelope derived from the host lipid bilayer containing the surface proteins: HA, NA and matrix protein 2 (M2)[32,33]. The inner core of the viral particle contains matrix protein 1 (M1), nuclear export protein (NEP, also named non-structural protein 2, NS2) and the viral genome. The virus genome is divided into eight segments of negative-single-stranded RNA (vRNA) coated by multiple subunits of nucleoprotein (NP), placed every twenty-four nucleotides, and attached to the heterotrimeric viral RNA-dependent RNA polymerase (RdRp) formed by PA, PB1 and PB2. This structure is the viral ribonucleoprotein complex (vRNP)[32–34] and is represented figure 1.2b. Ultrastructure inspection of transverse sections of virions highlighted the state of organization of segments that are arranged in the '7+1' conformation[31], shown in figure 1.2c.

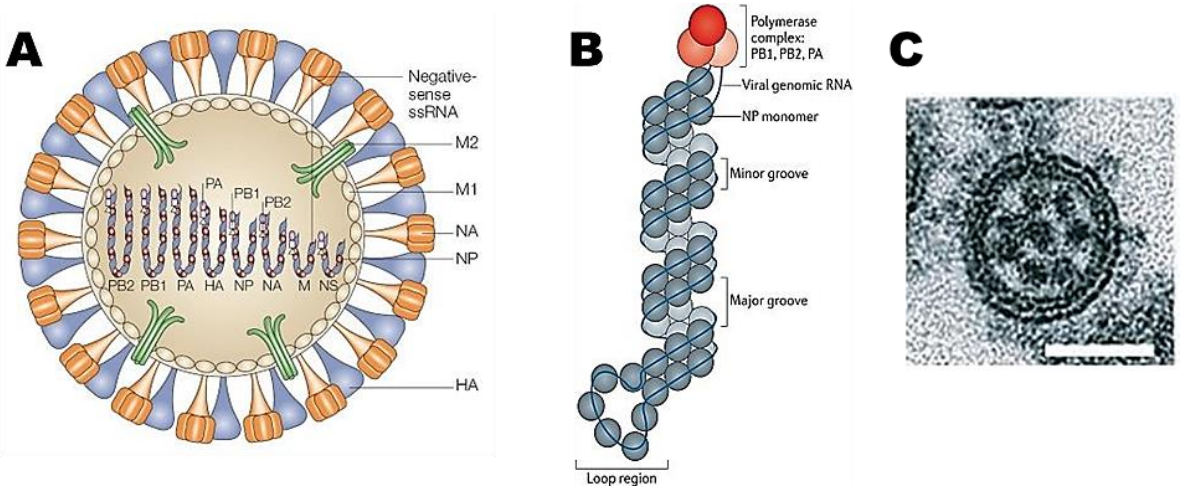

Figure 1.2. Influenza A virus. a) The viral particle has an envelope derived from the host lipid bilayer with surface proteins hemagglutinin (HA), neuraminidase (NA) and matrix protein 2 (M2). The core contains the segmented genome: eight segments consisting of negative-sense RNA coated with nucleoprotein (NP), and the viral polymerase complex[29]. **b)** Viral RNA is coated by NP at a ratio of 1NP:24nucleotides. The extremities are complementary and form a double-stranded structure, bound by the polymerase complex PA, PB1 and PB2. The segments adopt a cork-screw conformation with a loop region opposed to the polymerase[30]. **c)** Transverse section of a viral particle, with vRNPs in a '7+1' conformation[31]. Scale bar: 50 nm.

Despite coding for different proteins, as depicted below in table 1.3, all viral segments share the same organization. vRNAs have a middle antisense coding region flanked by short untranslated regions (UTR) at both ends. These UTRs are highly conserved and show partial complementarity, which leads to base pairing. The double-

stranded RNA that originates comprises the promoter sites where the viral polymerase is bound[35].

The eight segments encode for 10 essential proteins and several accessory proteins, whose expression is cell-type and strain dependent. In relation to our model influenza virus: A/Puerto Rico/8/1934 (PR8) H1N1, expression of viral proteins characterized thus far are shown in table 1.3.

Table 1.3. Genome segments and functions of coded peptides of H1N1 influenza A virus PR8 (A/Puerto Rico/8/1934)[36,37].

Segment	Size (bp)	Name of protein	Main function	Symbol	Start-stop (bp)	Protein length (aa)
1	2340	Polymerase basic subunit 2	5'-Cap recognition.	**PB2**	28-2307	759
2	2340	Polymerase basic subunit 1	RNA-dependent RNA polymerase.	**PB1**	25-2298	757
		Protein PB1-F2	Pro-apoptotic activity.*	**PB1-F2**	119-382	87
3	2230	Polymerase acidic protein	5'cap endonuclease	**PA**	25-2175	716
		Protein PA-X	Repression of RNApolI gene expression.*	**PA-X**	25-784	252
4	1780	Hemagglutinin	Binding to surface receptors; endosomal fusion.	**HA**	33-1733	565
5	1570	Nucleoprotein	Coating, nuclear export and replication of vRNAs.	**NP**	46-1542	498
6	1410	Neuraminidase	Cleavage of HA-receptor binding.	**NA**	21-1385	454
7	1030	Matrix protein 1	Matrix protein, nuclear export of vRNPs and viral budding.	**M1**	26-1007	252
		Matrix protein 2	Cytoplasmic vRNP release.	**M2**	26-784	97
		Matrix 42	Replaces M2 in adamantine containing media.*	**M42**		
8	890	Non-structural protein 1	Inhibition of interferon response.	**NS1**	27-719	230
		Nuclear export protein or Non-structural protein 2	vRNP nuclear export, along with M1 and NP.	**NEP or NS2**	27-864	121

*Auxiliary proteins.

1.3. Influenza A – replication cycle

A summarized overview of the viral lifecycle is depicted in figure 1.3. IAV enters the cell in an endosome and upon viral disassembly it releases its segmented genome to the cytoplasm. The eight segments are transported to the nucleus where they undergo transcription and replication. After *de novo* synthesis of viral genome and proteins, viral components are transported through the cytoplasm to the plasma membrane, where a new particle is assembled and buds out of the cell. The lifecycle can therefore be divided into viral entry, transcription and replication, and assembly which will be discussed in more detail below.

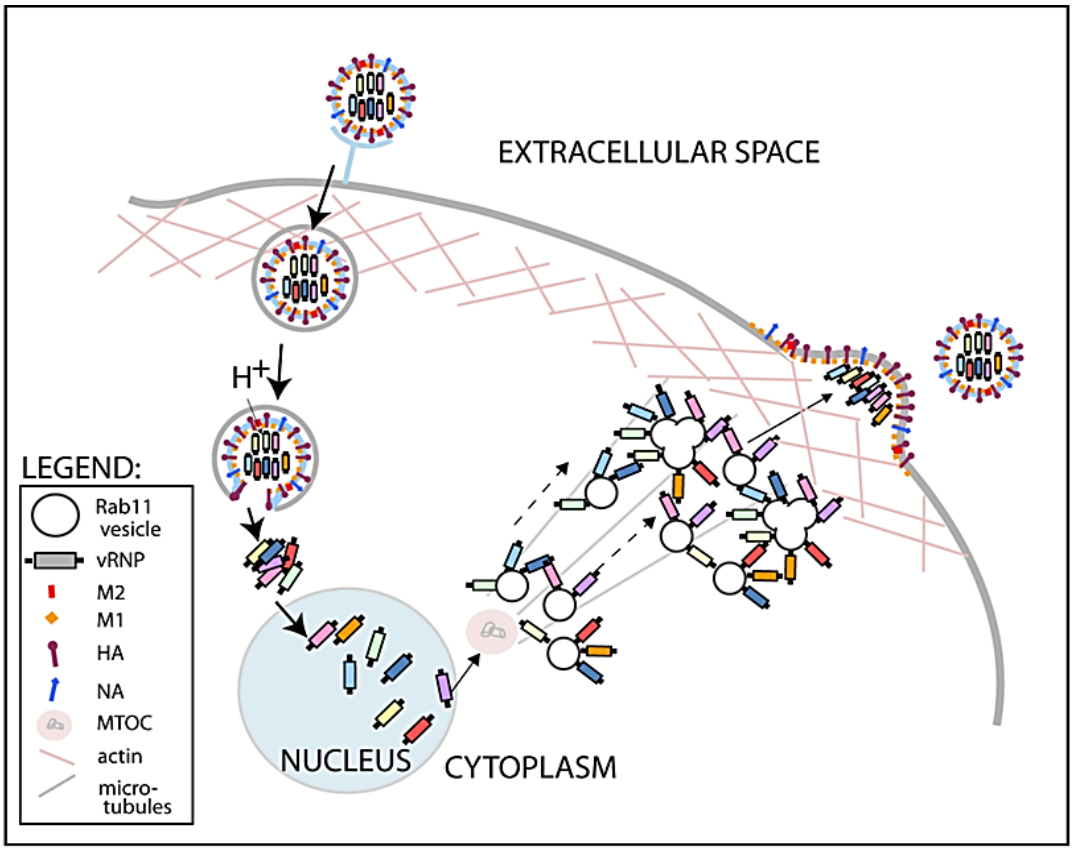

Figure 1.3. Influenza A virus replication cycle. IAV enters cells by endocytosis after binding of the viral protein HA to sialic acid residues at the plasma membrane. Following internalization, endosomal acidification results in the fusion between the virion and endosomal membranes, releasing vRNPs to the cytoplasm. After translocation of vRNPs into the nucleus, transcription and replication occurs, and new segments are exported to the cytoplasm. vRNPs accumulate near the microtubule organizing center, are loaded onto Rab11 vesicles and are transported through the recycling endosome toward the assembly sites at the plasma membrane. Each of the segments is then incorporated into a budding particle created with host membranes decorated with HA, NA and M2, and inwardly with M1. Illustration by MJ Amorim, unpublished.

1.3.1. Viral entry, disassembly and nuclear import

The virus enters cells through receptor-mediated endocytosis, via interaction of the viral protein HA with molecules of sialic acid present in glycoproteins at the cell surface[38]. The viral particle is endocytosed in both clathrin-coated and uncoated vesicles, indicating a versatility in the internalization routes[39]. During this process, the virus is transported from early to late endosomes, in actin and microtubule-dependent processes[40,41]. For releasing its contents, IAV exploits the endosomal system (figure 1.4) where the increasingly acidic pH, caused by the activity of ATPases during endosome maturation, triggers a conformational change in HA causing fusion of endosomal and viral membranes[42]. At this point, the low pH activates the proton pump activity of the viral protein M2 to acidify the virus inner core leading to the uncoating of the viral particle. This acidification contributes to weakening the affinity between matrix protein M1 and vRNPs, resulting in vRNP release to the cytoplasm[43].

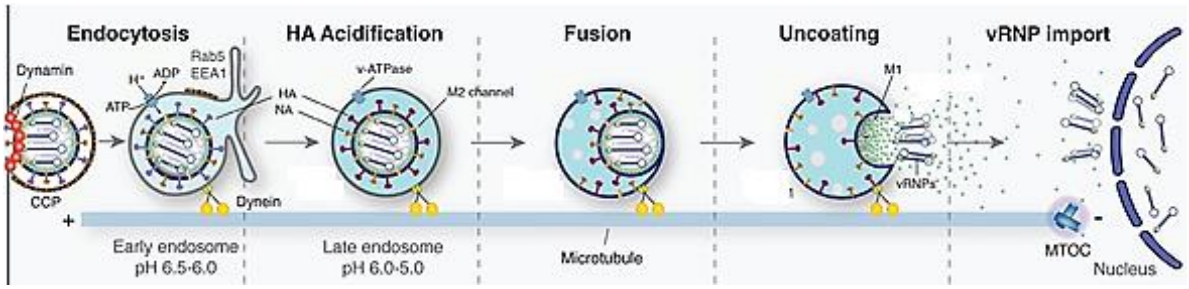

Figure 1.4. Viral entry by IAV. The virus enters cells by receptor-mediated endocytosis, by the binding of HA to sialic acid molecules present at the cell surface. Upon internalization, the increasingly acidic pH triggers a conformational change in HA causing fusion of endosomal and viral membranes. Afterwards, the increasing acidity spreads to the innercore of the particle, leading realtease of vRNPs to the cytoplasm. At this point, vRNPs move across nuclear pores into the nucleus to undergo transcription and replication[44].

vRNPs are then imported to the nucleus[33,45] to undergo transcription and replication. All vRNP proteins contain nuclear localization signals, but at this point, each segment relies only on the localization signals on NP to enter the nucleus[46]. Due to their large size, viral segments cannot diffuse passively, requiring passage through the nuclear pore, a process that relies on interactions with members of the importin superfamily: importins α1 and α5[47].

1.3.2. Genome transcription, replication and nuclear export

After nuclear import, negative sense vRNAs are the templates for production of both mRNAs to synthesize viral proteins and complementary RNA, the molecule that serves as template for *de novo* vRNAs synthesis[48].

Transcription is performed by the viral RdRp, resulting in 5′-capped and 3′-polyadenylated mRNAs[49,50]. However, both modifications, that occur to most cellular mRNAs, are attained by different mechanisms. Transcription begins with 'cap-snatching' of host-capped mRNAs (figure 1.5), a process mediated by the subunit of the viral polymerase PB2 that binds cellular mRNA 5'cap structures and presents these mRNAs to the subunit PA that cleaves them 10-13 nucleotides downstream[51]. Besides mimicking host mRNA in the cellular environment and being advantageous during translation, this structure also acts as a primer for polymerization of viral mRNA by the viral encoded RdRp. Elongation of viral mRNA (mRNA) proceeds by viral PB1, until it reaches a short polyU sequence located almost at the end of each segment[52]. Here, template RNA slips as the polymerase codes a longer polyA tail than its coding sequence by a stuttering mechanism[53],[52] until it is released. The viral mRNA thus is an incomplete complementary copy of vRNA as it terminates ~17 nucleotides upstream of the end of the RNA segment[54].

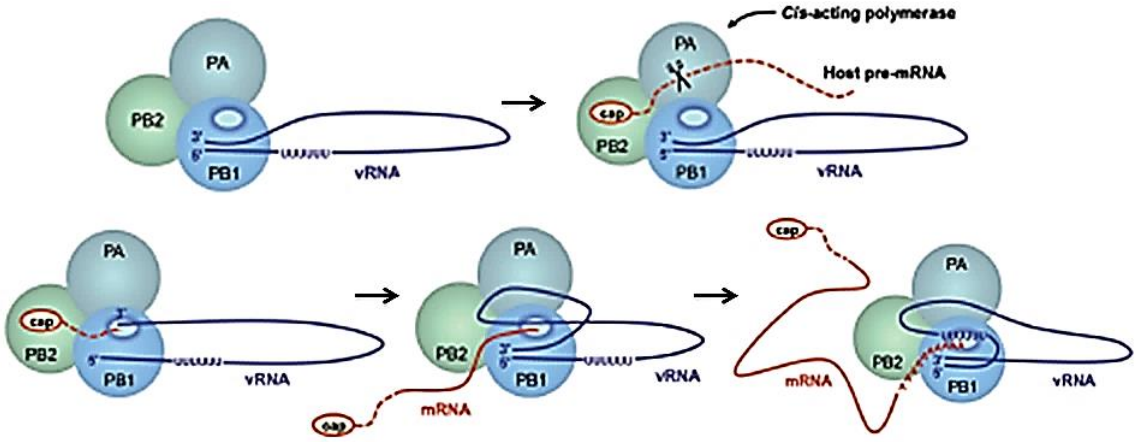

Figure 1.5. Events during IAV genome transcription. Each viral segment, bound to their own RdRp, starts by binding the 5'cap structures of cellular mRNAs via PB2. Then, PA cleaves the cap structure along with 10-13 nucleotides downstream, using it to prime the transcription of its viral mRNA. The elongation stage, performed by PB1, decelerates as the polymerase reaches a short polyU sequence at the 5' terminus of each segment. Due to a stuttering mechanism, a polyA sequence is synthesized with superior length than its own coding template. mRNAs from viral origin have similar modifications to cellular ones, but these are a result of different mechanisms. Adapted from[55].

As mentioned above, table 1.3 shows the viral proteins expressed from each segment upon infection with PR8. Several segments are capable of producing more than one protein, a diversity that is strain and cell-specific, and attained by different mechanisms. These mechanisms, indicated in figure 1.6, include: 1) multiple open reading frames (ORF), 2) alternative splicing or 3) ribosomal frameshift. This diversity increases the coding capacity of each vRNA for additional functional proteins. For instance, segment 2 has two different ORFs, one coding for viral polymerase subunit PB1 and another coding for the much smaller viral protein PB1-F2 (figure 1.6). While PB1 is the viral RNA polymerase, PB1-F2 has a different function. Expressed solely in specific cells, it localizes to the mitochondria and induces cell death[56]. Another example includes transcripts originating from segments 7 and 8 that can be alternatively spliced, a process that is accomplished by the host spliceosome complex. The alternatively spliced transcripts, M2 and NEP, obtained from segment 7 and 8, respectively, exist in lower abundance, than its intronless counterparts that code for M1 and NS1[48]. Another example of diversity is illustrated by segment 3 where a ribosomal frameshift results in a second protein PA-X[57]. The relevance of this protein is still to be understood, although mutant viruses lacking the peptide show reduced levels of replication and pathogenicity[58]. Other proteins have been identified, but require characterization during infection (M42[37], PA-N155 and PA-N182[58]).

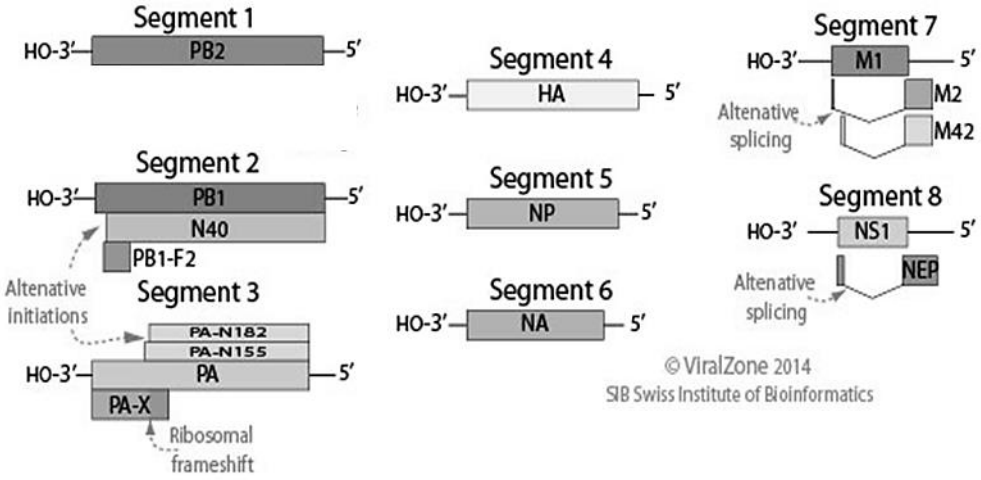

Figure 1.6. Representation of IAV proteins organized by segment. Variant proteins are noted with the corresponding molecular mechanism[59].

Upon translation, several viral proteins are translocated to the nucleus, including the viral polymerases and NP, necessary to form the progeny vRNPs[34].

As soon as there is a sufficient amount of vRNP-forming proteins, viral replication starts. The replication of the viral genome involves the synthesis of the intermediate, positive-sense, full length and complementary RNAs (cRNAs), that serve as templates for progeny vRNA synthesis, see figure 1.7a and b. Following synthesis, vRNPs need to be exported from the nucleus to reach the sites of virion assembly. Proteins M1 and NEP have nuclear localization signals and are responsible for nuclear export of vRNPs. These, along with vRNPs, organize a daisy-chain structure of vRNP-M1-NEP[60,61], and are carried to the cytoplasm through the cellular CRM1-dependent pathway[62–64].

The exit of *de novo* segments from the nucleus is not concomitant to segment replication. In fact, the virus has developed a way of timing the export from the nucleus by controling the amount of the NEP[65]. Only 10-15% of segment 8 transcrips code for NEP as a result of a weak splicing site which delays the synthesis and accumulation of the protein[66,67]. The remaining 85-90% of transcripts code for viral NS1 earlier in infection, that among other functions blocks interferon response[68]. This inhibition will allow vRNPs to better escape viral RNA host sensors on the way to the plasma membrane.

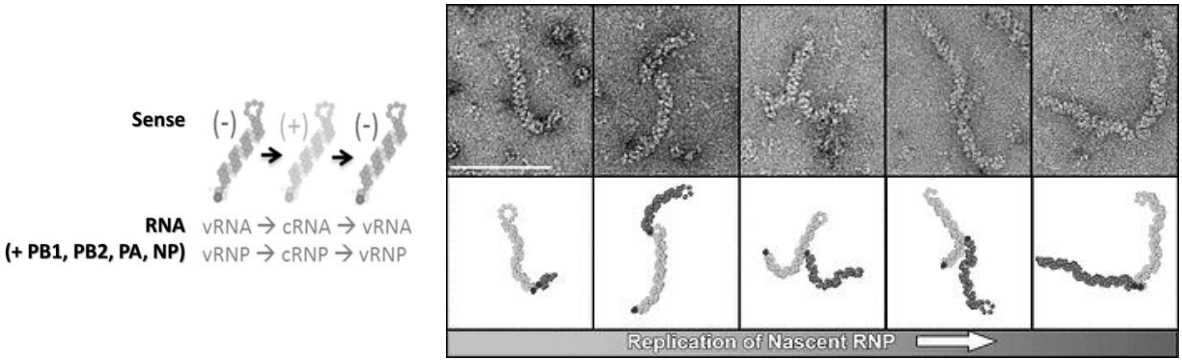

Figure 1.7. Replication of the viral genome. a) Schematic representation of viral replication. The viral genome synthesizes an intermediary positive-sense segment, in order to produce progeny negative-sense vRNP, in a second round of replication. **b)** Formation of 'nascent' vRNPs. Electron microscopy micrographs of negatively stained purified RNP with branched appearance[69].

1.3.3. Transport of the viral genome, assembly, budding and particle release

After nuclear export, the viral genome needs to reach the plasma membrane, where the viral particle assembles and buds out of the cell[32,34].

As summarized in figure 1.8a, the transport of vRNPs is at least a two-step process: first, in the proximity of the microtubule organizing center, vRNPs attach to vesicles bearing the small GTPase Rab11[70], a recycling endosome marker. Work by Kawaguchi and colleagues suggests that cytoskeleton-interacting protein YB-1 stimulates the delivery step of vRNPs to the recycling endosome[71]. Second, they are translocated using, in part, the microtubule network towards the plasma membrane. This way, vRNPs are directed from the perinuclear area through the recycling endosome, bound to Rab11 vesicles on route to the cell periphery. This process can be blocked by a drug called nucleozin[72], that "staples" NP molecules between different vRNPs, resulting in cytoplasmic aggregation of vRNP-Rab11-carrying vesicles[73], figure 1.8b. For detailed description on the mode of action of nucleozin see[72,73].

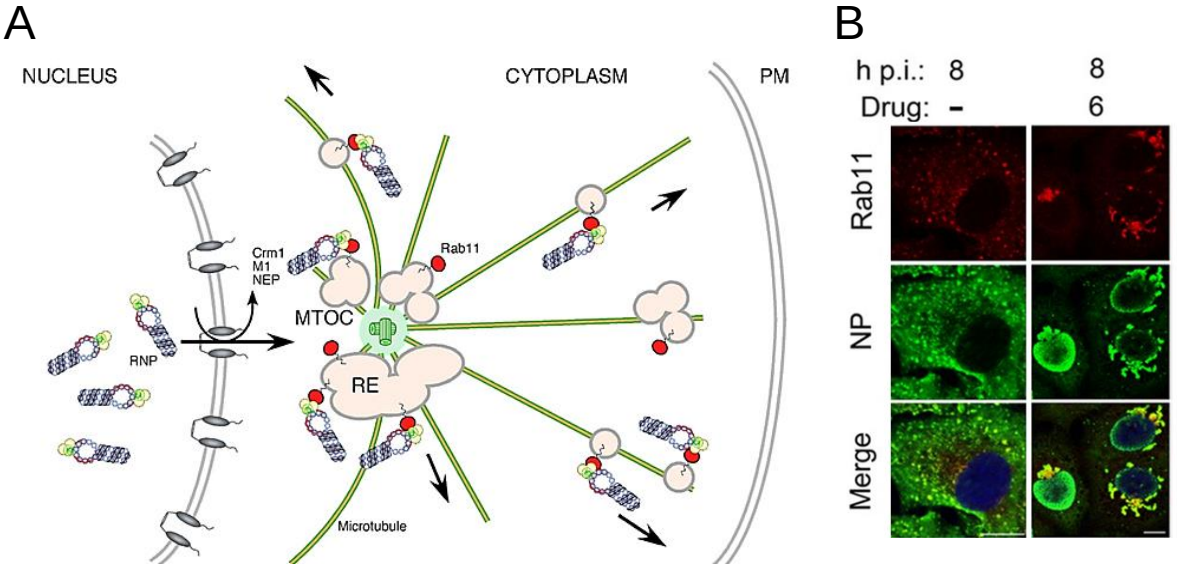

Figure 1.8. vRNP transport to the plasma membrane. a) After *de novo* synthesis and nuclear export, vRNPs are carried thorough the recycling endosome in Rab11-positive vesicles towards the plasma membrane[70]. **b)** Effects of nucleozin treatment in infected cells. Cytoplasmic vRNP (NP) aggregation co-localizes with Rab11 at 8 hours post infection in treated cells[73]. The drug added at 6 hours post infection at 1μM. Scale bar: 10μm.

Packaging of the eight segments, which is a necessary step to the production of infectious particles, does not seem to operate by a random mechanism[74,75] as production of infectious virions is more efficient than the 1/416 probability of combining eight

segments by chance[76]. Furthermore, the equimolar concentration of each segment in viral particles[77] even with unproportioned amounts in infected cells[78], reinforces the "selective packaging" model. The mechanism behind segment selection has been widely addressed and vRNP assembly has been suggested to occur directly by RNA-RNA interactions or through an unidentified protein intermediate[74] (figure 1.9a and b).

Literature postulates that different vRNP segments are carried together to the plasma membrane, still in a Rab11-dependent manner. In particular, studies by Chou et al.[79] and Lakdawaka et al.[80] proposed a model where vRNAs assemble on the way to the plasma membrane. They observed fusion/scission events between vesicles carrying vRNPs which resulted in co-localization of different segments. This raised the hypothesis that the recycling endosome may facilitate the assembly of the eight segments to be included in a virion, as illustrated by figure 1.9d.

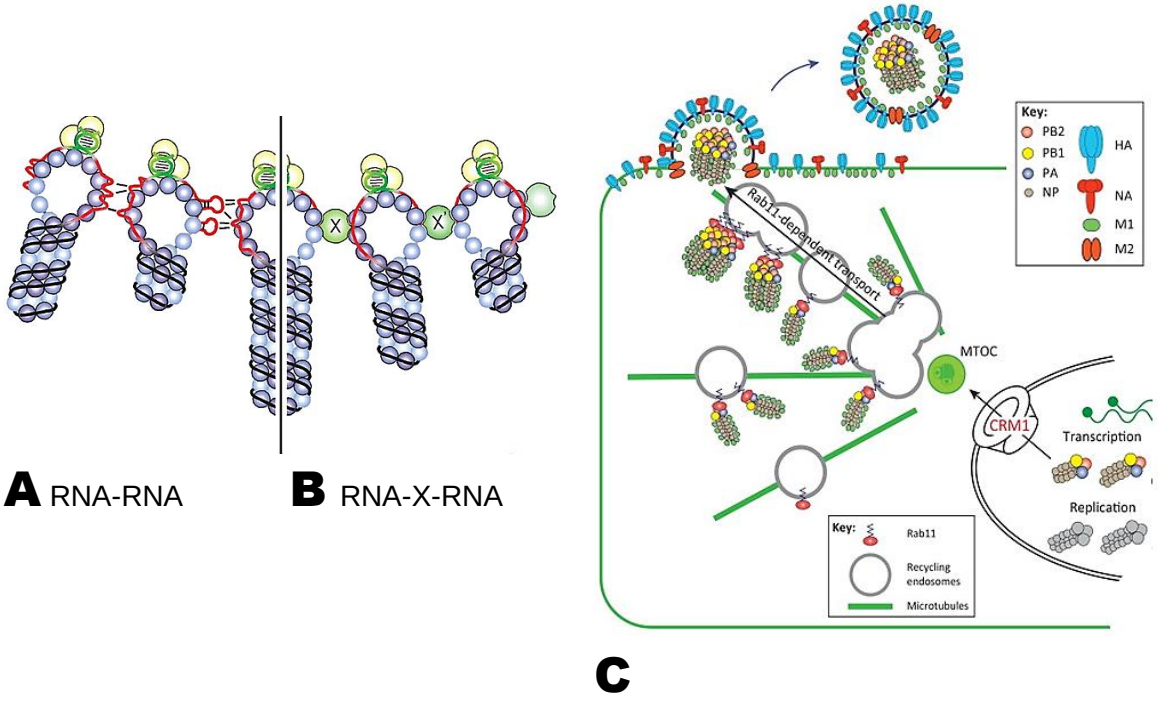

Figure 1.9. Selective packaging of IAV segmented genome. The assembly of a vRNP complex, containing each of the eight vRNAs, may be mediated by **a)** RNA-RNA interactions perhaps involved in secondary structures or **b)** by an intermediate host protein factor (X)[74]. **c)** Assembly and transport of vRNP complexes through the recycling endosome in Rab11 vesicles. Adapted from[81].

Our group has evidence that the vRNP binding to Rab11 vesicles competes with the standard ligation of Rab11-interacting proteins, FIPs, and causes "slowing down" in recycling efficiency (figure 1.10). In support, using correlative light and electron microscopy

our lab observed the coalescence of vesicles, resulting in enlarged aggregates (unpublished data). Such agglomeration of vesicles carrying different vRNPs allows for the close contact of segments, perhaps facilitating intersegment interaction. This notion agrees with previously established theories regarding the formation of vRNP super-complexes before reaching the plasma membrane, reviewed in[81]. In conformity, our data shows that transferrin recycling is impaired in infected cells, supporting a direct competition between Rab11 effectors and vRNPs.

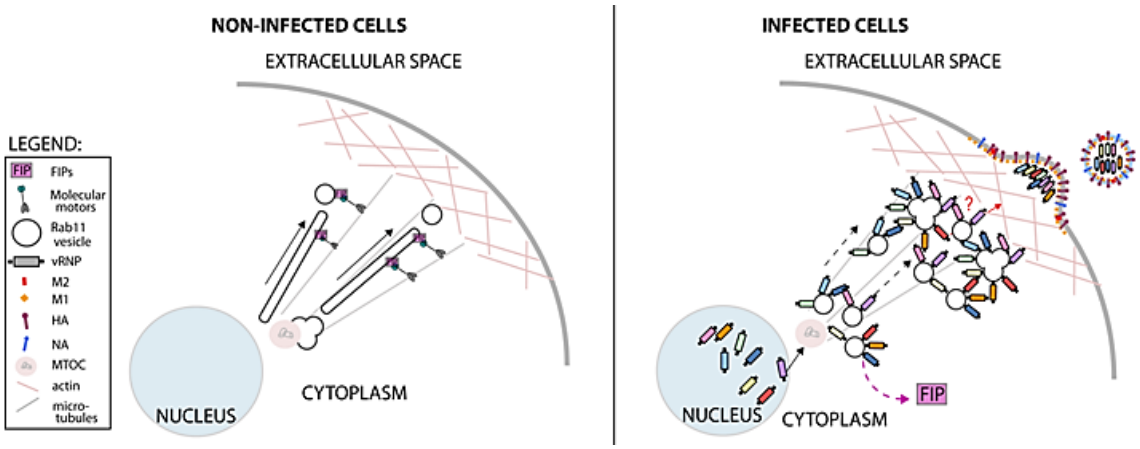

Figure 1.10. vRNP outcompete FIPs on the binding to Rab11, causing cytoplasmic agglomeration of vesicles carrying the viral genome. a) In non-infected cells, Rab11 binds to FIPs, allowing transport of these vesicles by molecular motors along the microtubule network. Whereas in **b)** infected cells, vRNPs outcompete FIPs, resulting in the cytoplasmic accumulation of vRNP containing vesicles. This event is thought to promote intersegment contacts, presumably aiding super-complexes formation, which are incorporated into a viral particle. Illustration by MJ Amorim, unpublished.

Regardless of whether in a complex or isolated, vRNPs need to meet the remaining viral proteins that localize beneath or at the plasma membrane. Viral assembly occurs at specific sphingolipid-enriched regions, called lipid rafts[32]. These are able to limit protein diffusion, operating as functional domains for example by harboring many proteins involved in signaling cascades[82]. Viral envelope proteins HA and NA are targeted to these regions, conversely to M2, which is resides in regions flanking lipid rafts[83]. The viral protein M1, mentioned above to participate in the nuclear export of vRNPs, also ensures that vRNPs do not return to the nucleus[84]. Furthermore, it has also been suggested that M1 plays a part in particle assembly by bridging the virion core to the envelope, especially the viral protein M2[85], although binding to HA and NA might also occur[86]. However, the means by which M1 is transported to the assembly sites remains undescribed.

The process of viral budding is still unclear, but requires the following steps: 1)

induction of membrane tension and curvature leading to the formation of a bud, 2) elongation of the particle, and finally 3) recoiled membrane curving resulting in membrane scission and release of the particle[26]. It is generally agreed that curvature is facilitated by binding of the matrix protein M1 to the cytoplasmic tails of envelope proteins HA and NA microdomains, although binding domains between these proteins remain to be identified[34,87]. This is thought to induce stiffness in the membrane, resulting in a small curvature[34,88]. Of note, each one of these proteins has individually produced viral-like particles in *in vitro* assays, suggesting a synergistic role in promoting viral budding and release[34]. Subsequently, the bend may be elongated by the action of M1, which also associates with the viral genome[60], perhaps prompting segment packaging. Lastly, ion channel M2, which is excluded from lipid-rafts, has an important role forming a neck structure by the insertion of an amphipathic helix into the lipid bilayer resulting in scission of membranes[34]. This process of scission is, in many enveloped viruses, attributed to host's ESCRT proteins. However, IAV bypasses the need for ESCRT proteins, being only mediated by viral M2[89].

There are however several other host factors that have been suggested to influence the budding process. Among these are: F1Fo ATPase, thought to influence membrane bending by contributing with mechanical energy by hydrolysis of ATP[90]; actin modulating protein Cofilin-1 by influencing cytoskeleton organization needed for efficient budding[91]; RACK1, shown to be involved in cytokinesis and to bind the viral protein M1 to facilitate viral release[92]; Annexin-A6 involved in cholesterol homeostasis that was suggested to affect viral release[93]; and CD81, involved in signal transduction, whose depletion resulted in abnormally elongated virions attached to the plasma membrane[94].

To be released, the virus requires a couple of significant last steps to complete its life cycle. Firstly, it needs the action of the viral envelope protein NA to cleave the HA-sialic acid bond established at the cell surface during budding[95,96]. After particle release, the virus undergoes one last step of maturation, by cleavage of viral protein HA by extracellular proteases[97,98]. Without this modification the next round of infection would be unsuccessful, as HA would not mediate membrane fusion between endosomal and virus membranes upon entry[97].

1.4. Cellular secretory pathway and vesicle trafficking

As an obligatory intracellular parasite, viruses typically highjack cellular machinery and pathways to complete their replication cycle. In the case of IAV, the cellular secretory pathway is indispensable for assembly of progeny virions[70,99], as most viral components reach the plasma membrane on account of this system to assemble into a particle. As described in the previous section, the newly-synthesized viral genome, in form of vRNPs, is loaded onto Rab11 vesicles and carried to the plasma membrane[70]. Rab11 is a major regulator of the recycling endosome. This organelle consists of networks of tubules of 60 nm wide that emanate from the microtubule-organizing center, transporting endocytosed or newly synthesized molecules to the plasma membrane[100]. Figure 1.11 shows the communication web of the recycling endosome with the remainder of the secretory pathway. Recycling receives material from the early endosome and also from the trans Golgi network (TGN).

Protein sorting is carefully regulated with high specificity. Events of mistargeted proteins are the basis of many neuropsychiatric, endocrine and metabolic disease pathogenesis[101]. Secretory pathway dynamics are coordinated mostly by small GTP-binding proteins[102,103]. This superfamily has hundreds of known proteins divided into five families: Ras, Rho, Ran, Rab and ADP-ribosylation factors (Arf); the nomenclature guidelines indicate that all-capital letters should be solely used when referring to human Arf proteins. In a simplistic way, the Ras family is generally responsible for cell proliferation, Rho for cell morphology, Ran for nuclear transport and, the focus of our work, Rab and Arf proteins for vesicle transport[102].

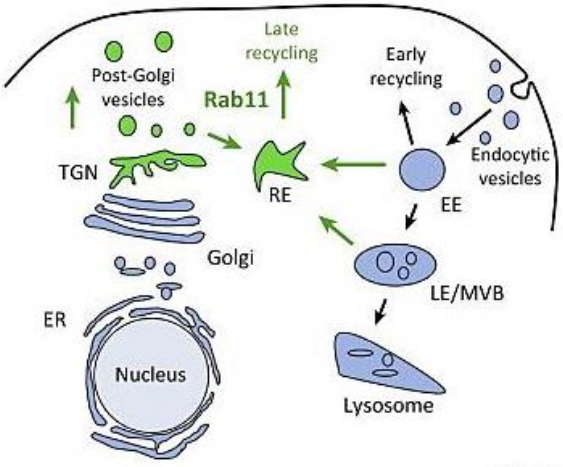

Figure 1.11. Rab11 as the major regulator of the Recycling Endosome. Rab11 orchestrates the molecule transport originating from the trans Golgi network (TGN), early or late endosomes (EE, LE) towards the plasma membrane, routes highlighted in green. Adapted from[100].

In the context of vesicular trafficking between organelles, Rab proteins are thought to dictate the destiny of the cargo. Every other event needed to achieve the formation of a vesicle, requires the participation of many other molecules, recruited or removed by a complex and dynamic flow operating in sequential order.

In very simplified terms, that are depicted in figure 1.12, a budding vesicle starts forming in a donor compartment, composed of specific lipids as a result of the activity of lipid modifying enzymes[104]. These work as docking platforms for Arf family activating proteins, the guanine nucleotide exchange factor (GEF)[105]. Each GEF protein activates its corresponding Arf by switching GDP to GTP, a process described later on. Arfs recruit coating molecules to the surface of the budding vesicle, cargo from the cytoplasm and RabGEF proteins able to recruit and activate Rabs, constituting a signaling cascade of events[106]. Each organelle has a specific set of Rab proteins that dictate its identity and consequent function[107]. Subsequently, Rabs are in turn able to attract molecular motors that transport vesicles along the cytoskeleton to acceptor membranes, where they fuse[108]. Tethering factors are responsible for attachment of vesicles to membranes, as other proteins facilitate fusion between vesicles and the target membrane, collectively called SNAREs[109].

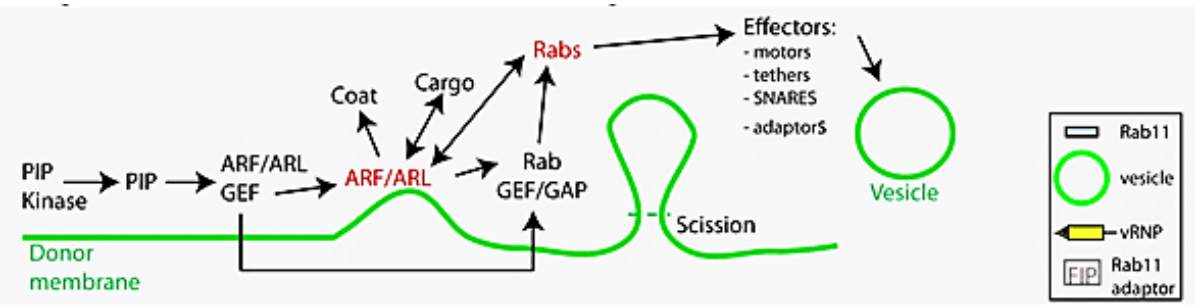

Figure 1.12. Biogenesis process of a vesicle during intracellular trafficking. Vesicle formation involves a series of sequential steps with the intervention of several classes of proteins. Phosphoinositide kinases modify lipids able to anchor and recruit proteins necessary for vesicle formation. Initially, ARF/ARLs recruit coating and scission factors as well as cargo. Then, Rabs are responsible for attraction to motors, tethering, docking, fusion of vesicles with the donor compartments/membranes[110].

Interestingly, some RabGEFs were found to be recruited by Arf GTPase activating proteins (Arf-GAPs)[111], some ARFs by Rab effectors[112] and some ARFs attracting lipid-modifying enzymes[113], suggesting a more complicated network of interactions between all these individually described family of proteins.

The highjack of the recycling endosome by IAV can be inhibited by depleting cells from Rab11, with severe effects on viral production. Given the complexity of the secretory

pathway, it is anticipated that other host factors are involved in the trafficking of Rab11 vesicles, thus affecting vRNP transport towards assembly sites.

The ARF family is a subset of the small GTPase superfamily with important roles in vesicular traffic, as described below. In total, it comprises: 5 ARFs, 21 ARF-Like proteins (ARLs), two SAR1 isoforms, a ARF-related protein 1 (ARFRP1) and TRIM protein 23 in humans[114–116].

ARF proteins acquired their name on account of their role as co-factors in the catalysis of ADP ribosylation, by the cholera toxin[117]. Currently, the ARF reference is kept, but only ARFs share the co-factor capacity for the toxin action, as the remaining members of the family do not promote ADP ribosylation[118]. Instead, ARLs and SARs are part of the ARF-family not based on specific functions, but due to sequence comparison and structure similarity. The sub-category of ARLs arose from the discovery of hypothetical ARF sequences with identity below 60%, that lacked the co-factor activity for cholera toxin and were unable to rescue lethal mutants of arf1- and arf2- deletion in *S. cerevisea*[115,118]. Additionally, SAR1 was one of the earliest members of this family, with a name derived from its identification as a secretion-associated Ras-related protein. In comparison to ARFs, SAR1 isoforms present a sequence identity inferior to 30%[118].

Consistent with the remaining small GTPases, ARF-family proteins generally are able to interconvert from an inactive GDP-bound to an active GTP-bound state and to bind specific effectors while in the “on” or “off” status. The GDP/GTP switch is generally very slow, requiring catalysis by GEFs, as mentioned and although belonging to the small GTPase superfamily, have a negligible GTPase activity and rely on GAPs to be inactivated[115,119].

ARF-family proteins share distinct signatures in its amino acid sequence, associated with functional domains. Firstly, they have an N-terminus amphipathic helix that undergoes post-translational modifications, functioning as an anchor to membranes when the protein is activated by GEFs[115,120] (figure 1.13a and c).

Secondly, members from the ARF-family have specific domains, which change configuration upon activation/inactivation, termed switch-1 and switch-2 (figure 1.13b). These regions flank a two β-strand interswitch domain, which ultimately rearranges switch 1 and 2[115,119]. In its GDP-bound inactivated state, the protein is soluble due to the N-terminus helix being packed into a hydrophobic groove on the opposite side of the protein.

Here, an aspartate residue of the interswitch mimics the charge of GTP, preventing the binding of the molecule. Upon activation with a GEF, the strands of the interswitch slide pulling switch 1 and 2 'up' and projecting out the amphipathic helix[119,121]. Simultaneously, the switch regions acquire the GTP-binding conformation, resulting in an activated protein, with an exposed helix to bind membranes. Membrane dissociation occurs spontaneously upon GTP hydrolysis, upon the action of a GAP[116].

Exceptions include ARF6, which remains membrane-bound in its off-state, perhaps interacting with other membrane-localized partners mediating signaling[122].

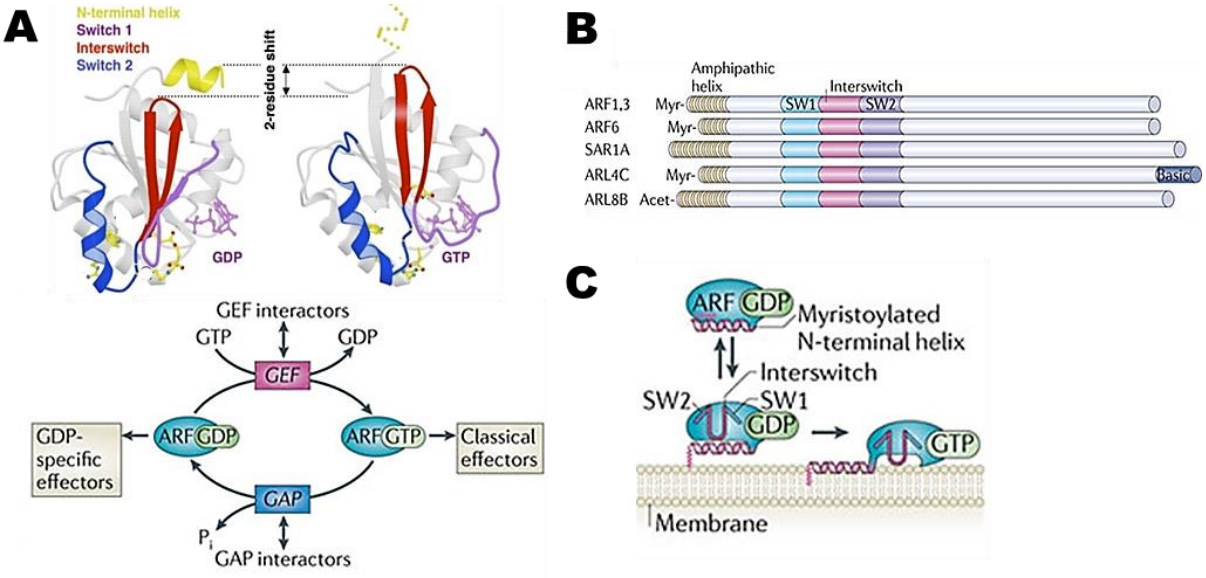

Figure 1.13 Activation cycles of ARF proteins. a) GDP/GTP bound alternative conformations of ARF1[118] and mechanisms of interaction with ARF GEFs or GAPs[115]. **b)** Domains conserved in ARF/ARLs[115]. **c)** GTP-bound conformation involves recruitment to a specific membrane[115].

Thirdly, the spacer sequence between the helix and the remaining ARF is rather short in comparison with the one from Rabs or Rhos, placing them in closer proximity to membranes in its activated state[115,116]. This feature was initially associated with the participation of ARFs in vesicle biogenesis, having coat proteins or lipid modifying enzymes as effectors, shaping or attracting the bilayer surface[116,123]. This participation in the early steps of vesicle budding, also shared by SAR1 isoforms, has been broadened to include additional functions such as involvement in: microtubule dynamics (ARL2[124,125]), cell cycle progression (ARL3[126]) or to influence organelle positioning (ARL8[127]).

Given their importance in membrane traffic regulation, our aim is to identify members of the ARF-family of proteins involved in the trafficking of the viral genome towards the plasma membrane and to characterize their role in this process.

1.5. Objectives of the work

Infections due to IAV in humans cause disease of variable outcomes including excess death rates. Existing strategies aim to prevent epidemics and pandemics with vaccination and mitigate the effects of infections with drugs that inhibit viral proteins. However, antiviral medication leads to the emergence of drug-resistant escape mutants, rendering inefficient the scarce amount of treatments available for IAV infection. Thus, novel antivirals are needed. An alternative approach to targeting viral proteins in IAV therapy would be to inhibit key host processes involved in viral replication. Blocking the activity of cellular proteins or its interaction with the virus requires in-depth knowledge of host-pathogen interactions.

The assembly of virions is a crucial step in the viral lifecycle. In particular, the transport of the viral genome to assembly sites has, as explained in the introduction, emerged as key in viral replication for a variety of reasons. The recycling endosome, and its major regulator Rab11, were found to influence this process, but no other host proteins were identified. The secretory pathway is notorious for its complexity, with specific networks of proteins securing vesicular biogenesis, transport and delivery to precise destinations. This complexity makes it unlikely that Rab11, the only protein thus far implicated in the process, may coordinate trafficking of vRNPs alone. One of the most prominent families that regulate the secretory pathway is the ARF-family. The goal of this project is to expand on host requirements for the recycling endosome and identify which ARFs are important for viral infection.

To this end, an initial screen, herein described in the preliminary data section, identified a promising candidate to influence IAV infection: ARL15. The aim of this work is to characterize the role of ARL15 during infection with IAV. This thesis is divided into two main subchapters of results where the following topics will be assessed:

I. The effect of ARL15 depletion on IAV production;
II. The levels, intracellular distribution and function of ARL15 during IAV infection.

Altogether, this study aims to identify novel host-factors involved in IAV infection and shed some light on the mechanisms that lead to an efficient assembly of IA virions. This constitutes the first step in understanding whether a specific pathway could be targeted for antiviral therapy.

CHAPTER 2 | Materials and methods

Table 2.1. Reagents. Primary and secondary antibodies, siRNAs, plasmids, transfection and cloning reagents used in the procedures described below.

Primary Antibodies	Brand, Reference	Host	Dilutions
ARL15	ProteinTech®, #11934-1-AP	Rabbit	Western blot: 1:500 Immunofluorescence: 1:100
GAPDH	Sicgen®, #AB0049-200	Goat	Western blot: 1:2000
GBF1	BD transduction Lab®, #612116	Mouse IgG1	Immunofluorescence: 1:500
GFP	Sicgen®, #AB0066-200	Goat	Western blot:1:5000
HSP 60	AbCam®, #ab31115	Rabbit	Immunofluorescence: 1:200
Myc	AbCam®, #ab9132	Goat	Western blot: 1:500
NP (Ms)	AbCam®, #ab20343	Mouse IgG2a	Immunofluorescence: 1:2000
NP (Rb)	Homemade, *in*[70]	Rabbit	Western blot: 1:1000; Immunofluorescence: 1:1000
Rab11	Invitrogen®, #715300	Mouse	Immunofluorescence: 1:100
TOM 20	Sigma®, #WH0009804M1	Mouse IgG1	Immunofluorescence: 1:100

Secondary Antibodies	Brand, Reference	Host	Dilutions
Alexa Fluor® Anti-Rabbit 488	Life technologies®, #A-11008	Goat	Immunofluorescence: 1:1000
Alexa Fluor® Anti-Mouse 488	Life technologies®, #A-11001	Goat	Immunofluorescence: 1:1000
Alexa Fluor® Anti-Mouse IgG2a 488	Life technologies®, #A-21131	Goat	Immunofluorescence: 1:1000
Alexa Fluor® Anti-Rabbit 568	Life technologies®, #A-21069	Goat	Immunofluorescence: 1:1000
Alexa Fluor® Anti-Rabbit 568	Life technologies®, #A-21069	Goat	Immunofluorescence: 1:1000
Alexa Fluor® Anti-Mouse IgG1 647	Life technologies®, #A-21240	Goat	Immunofluorescence: 1:1000
IRDye 800CW Donkey Anti-Goat	Li-Cor®, #926-32214	Donkey	Western blot: 1:10 000
IRDye 800CW Donkey Anti-Rabbit	Li-Cor®, #926-32213	Donkey	Western blot: 1:10 000
IRDye 680RD Donkey Anti-Rabbit	Li-Cor®, #926-68073	Donkey	Western blot: 1:10 000

siRNAs	Brand, Reference	Concentrations
siNT (Non-targeting)	Quiagen , #SI1022076	Final concentration: 25nM
siARL15-1, -2, -3	Quiagen , #SI04160366; #SI04165098; #SI04206258	Final concentration: 25nM
siGFP	Quiagen , #SI04380467	Final concentration: 25nM

Transfection Reagents	Brand, Reference	Concentrations
Lipofectamine® 2000	Life technologies®, #11668027	Final concentration: 0.15% (v/v)
Lipofectamine® LTX	Life technologies®, #15338100	Final concentration: 0.10% (v/v)
DharmaFECT-1	Dharmacon®, #T-2001	Final concentration: 0.20% (v/v)

(continuation of Table 2.1)

Cloning Reagents	Brand	Specifications
Primer A1	Eurofins	Forward primer, with an AgeI restriction site and the initial coding sequence of ARL15. (5'accggtatgtctgatctccga)
Primer A2	Eurofins	Reverse primer, with a BamHI restriction site and the terminal ARL15 coding sequence followed by a myc tag. (5' ggatcccagatcctcttctgagatgagtttttgttccattcttacagcttc)
Primer B1	Eurofins	Forward primer, with an AgeI restriction site and a myc-tag followed by the initial coding sequence of ARL15. (5'accggtatggaacaaaaactcatctcagaagaggatctgatgtctgatctccga)
Primer B2	Eurofins	Reverse primer with a BamHI restriction site and the terminal coding sequence of ARL15. (5' ggatcctcacattcttacagcttcatggtc)
Primer C1	Eurofins	Forward primer with a BamHI restriction site followed by initial coding sequence of Bcl-2 mitochondrial sorting signal. (5' ggatccttctcctggctgtctctgaa)
Primer C2	Eurofins	Reverse primer with the terminus coding sequence of Bcl-2 mitochondrial sorting signal followed by a BamHI restriction site. (5' ggatcctcacttgtggcccagatagg)
AgeI	New England Biolabs, #174R0552S	10 units per reaction
BamHI	New England Biolabs, #174R3136S	10 units per reaction
NheI	New England Biolabs, #174R0131S	10 units per reaction
Quick Ligase	New England Biolabs, #174M2200L	10 units per reaction
NZY miniprep kit	NZYtech, #MB01002	Used according to manufacturer's instructions

Plasmids	Description	Source
pGFP	pEGFP-N1 with resistance to kanamycin, expressing an EGFP fluorescent tag under a CMV promoter.	Invitrogen©
pARL15-GFP	ADP Ribosylation factor 15 coding sequence, in a pEGFP-N1 backbone, with resistance to kanamycin, expressing ARL15 with a C-terminal fluorescent tag, under a CMV promoter.	Kindly given by J Mota – ITQB
pARL15-myc	ADP Ribosylation factor 15 coding sequence, in a pEGFP-C1 backbone, with resistance to kanamycin, expressing ARL15 with a C-terminal myc tag, under a CMV promoter.	A Nascimento
pMyc-ARL15	ADP Ribosylation factor 15 coding sequence, in a pEGFP-C1 backbone, with resistance to kanamycin, expressing ARL15 with a N-terminal myc tag, under a CMV promoter.	A Nascimento

(continuation of Table 2.1)

pMitoCherry	Tom20 mitochondrial sorting signal cloned in the N-terminus of mcherry in pmCherry-C1 plasmid with resistance to kanamycin, under a CMV promoter.	M Alenquer – CBV, IGC
pMitoRab11a-DN	Tom20 mitochondrial sorting signal cloned in the N-terminus of pCherryRab11a-DN plasmid with resistance to kanamycin, under a CMV promoter. Rab11a has with single substitution in S25N.	A Seixas – CBV, IGC
pMitoRab11a-WT	Tom20 mitochondrial sorting signal cloned in the N-terminus of Rab11 in pCherryRab11a-WT plasmid with resistance to kanamycin, under a CMV promoter.	A Nascimento
pARL15-myc-mito	Bcl-2 mitochondrial sorting signal cloned in the C-terminus of ARL15-myc sequence of pARL15-myc, with resistance to kanamycin, under a CMV promoter.	A Nascimento
pSAR1A-GFP **pSAR1B-GFP**	Coding sequence of Secretion-Associated Ras proteins A and B isoforms (Sar1A and Sar1B) inserted in pEGFP-N1, with resistance to kanamycin, under a CMV promoter.	B Kellen – CBV, IGC
Plasmids expressing the coding sequence of: ARF1, ARF3, ARF4, ARF5, ARF6, ARL1, ARL2, ARL3, ARL4A, ARL4C, ARL4D, ARL5A, ARL5B, ARL8A, ARL8B, ARL9, ARL10, ARL13B, ARL14, ARL16 and ARL17), ARF-related protein 1 (ARFRP1), and tripartite motif-containing protein 23 (Trim23) under a CMV promoter, inserted in a pEGFP-N1 backbone (GFP tag on the C-terminus) and resistance mark to kanamycin.		Kindly given by J Mota – ITQB

Cell Lines | Different cell lines were used according to specific purposes. HeLa cells, originated from cervix adenocarcinogenic epithelia, are easy to transfect and suitable for immunocytochemistry assays, due to their expanded shape. Madin-Darby canine kidney (MDCK) epithelial cells have high adherence to substrate. Therefore, MDCKs are more resistant to the presence of trypsin, and were used in assays involving viral titration by plaque formation. Human alveolar basal epithelial (A549), originating from lung carcinoma, were used as an *ex vivo* model for IAV infection. Human embryonic kidney 293T (HEK 293T) epithelial cells were used when high transfection efficiency was required.

Stable Cell Lines | A549 and HEK 293T cells were transduced individually with lentivirus encoding GFP tagged ARL15, Rab11a WT or Rab11a variants containing the point mutations Q70L(constitutively active (CA)) or S25N (dominant negative (DN)). These stable cell lines will be henceforward addressed as 'ARL15-GFP', 'GFP-Rab11a-WT', 'GFP-Rab11a-CA', 'GFP-Rab11a-DN', respectively. As background, a control cell line expressing GFP protein was established, and will be designated 'GFP' stable cell line throughout the text.

Cell Culture | All cell lines were cultured accordingly to[128] in Dulbecco Modified Eagle medium (DMEM) (Life Technologies), supplemented with 10% fetal bovine serum (V/V), 200 mM glutamine, 100 U/ml penicillin and 10 µg/ml streptomycin. Stable cell lines described above were also supplemented with 1.25 µg/mL puromycin for positive selection. Whenever mentioned, nucleozin, diluted in DMSO, was added at 2µM.

Infection | All infections were carried out with reverse genetics-derived A/Puerto Rico/8/34 (PR8; H1N1)[129] produced as in[130]. PR8 was added at the multiplicity of infection (MOI) specified in each case, in serum-free DMEM (Life Technologies) or in OptiMEM Reduced Serum Media (Life Technologies) in case of infection of transfected cells. After 30 min of infection, cells were overlaid with serum free DMEM media supplemented with 0.14% (w/v) bovine serum albumin (BSA).

siRNA silencing | 10^5 A549, or A549 stably expressing 'ARL15-GFP' or 'GFP' were transfected with Flexitube siRNA (Qiagen) targeting: 'GFP' (SI04380467), and/or the 3' untranslated region of endogenous ARL15 (SI04160366, SI04165098, SI04206258), using Dharmafect-1 transfection agent according to manufacturer's instructions. As a negative control, a non-targeting RNA (SI04380467) sequence was used. Cells were incubated at 37^0C and 5% CO_2 for 36 hours prior to being infected with PR8 at a MOI of 5. Cells were harvested at 16h p.i. and processed for immunofluorescence, plaque assays and/or western blotting.

Rescue Assays | 10^5 HEK 293T cells were transfected for 36h with siRNAs targeting ARL15 or control siNT, concomitantly with 200 ng of the following plasmids: pARL15-myc, pARL15-GFP and pGFP using Lipofectamine®2000 according to manufacturer's guidelines. Cells were infected with PR8 (MOI of 5) and incubated for 16 hours at 37^0C and 5% CO_2. After this time, supernatants were collected for plaque assays and cells were lysed in Laemmli buffer for western blotting.

Plasmid transfections | 10^5 HeLa cells were transfected with 200ng of plasmid using Lipofectamine LTX, according to the manufacturer's instructions, and incubated for 24h. Then cells were infected, as explained above, with indicated MOI and incubated for a referred period of time until being fixed in 4% PFA before immunofluorescence processing.

Plaque Assays | In order to quantify virus titers, a confluent monolayer of MDCK cells was infected with 1:10 serial dilutions of each supernatant sample (10^{-1} to 10^{-6}) in serum free media. One hour post-infection cells were overlaid with a solution diluted 1:2 in serum free media containing 4% Avicel, 0.14% BSA, 1µg/mL *TPCK* trypsin, and incubated at 37^0C, 5%CO_2 for 36 hours. Then, cells underwent a fixation-staining step in a 4%PFA-0.2% toluidine blue solution. Virus titers were estimated as plaque forming units/mL (PFU/mL).

Western Blot | Approximately 10^4 cells kept in Laemmli buffer and separated by SDS-PAGE, were transferred to a nitrocellulose membrane at 200 mA for 45 minutes. A two buffer system was used in stacks containing filter paper, the membrane and the gel: starting at the negative pole, 3 layers of filter paper soaked in 0.3M Tris and 20% (v/v) ethanol followed by 3 layers of 25mM Tris and 20% ethanol (v/v) were laid below the nitrocellulose membrane. Then, the acrylamide gel was placed over the membrane, followed by another 6 layers of filter paper in 25mM Tris and 20% (v/v) ethanol, under the positive pole. Upon transfer, membranes were blocked in 5% skimmed milk for 30 min in 0.2% (v/v) tween-PBS (PBST). Then, membranes were incubated with primary antibodies against the proteins of interest for 1 hour followed by extensive washing in PBST. Membranes were then incubated with host-specific secondary antibodies conjugated to fluorochromes LiCor 800 or 680 for 30 minutes and washed three times in PBST. Both incubations were done at room temperature. Membranes were scanned using a LiCor Biosciences Odyssey near-infrared platform.

Immunofluorescence | Approximately 10^4 cells were seeded on 13 mm diameter glass coverslips (VWR), infected, and/or transfected as described above. Upon the time p.i. required, cells were fixed in 4% (v/v) paraformaldehyde for 20 minutes, washed in 0.5% (w/v) BSA-PBS and permeabilised in 0.2% Triton X-100-PBS for 7 minutes. Upon this time, cells were blocked in 0.5% (w/v) BSA-PBS. Primary antibody staining was performed against proteins of interest for 1 hour followed by secondary staining using host-specific conjugated antibodies Alexa 488, 647 or 568 incubated in the dark, for thirty minutes. Washes between stainings were performed thoroughly with 0.5% (w/v) BSA-PBS for 15 minutes at room temperature to remove traces of unbound antibody. Coverslips were mounted using Dako© mounting medium. Confocal images were acquired on a Leica SP5

confocal using a 63x 1.3NA Oil immersion objective, and illuminated with Ar, HeNe or UV lasers. From fixation onwards, the procedure was carried out at room temperature.

Measurement of vesicular area | Confocal images stained with NP were analyzed using Fiji 'Analyze Particles - Area' tool. The output value of the area of each vesicle was used to calculate an average vesicular area per cell. The mean value per cell was plotted and evaluated for statistical significance using the methods described below. A minimum of 20 cells were analyzed per condition.

Co-localization analysis | Confocal images were analyzed using Fiji plugin 'Colocalization Finder', to determine areas of overlap between indicated stainings. The output value of Pearson's Correlation Coefficient was acquired for twenty cells per condition, plotted and evaluated for statistical significance.

Statistical analysis | Results are expressed as mean ± standard error of the mean (SEM). Exceptionally and as indicated, dot plots containing measurements of either colocalization or vesicle size, were expressed as median, since these had already taken into account the average value per cell. D'Agostino Pearson test was performed to assess the normal distribution of values. Statistical significance analysis was conducted by the one way analysis of variance (ANOVA) or by unpaired t-test, with 95% confidence. Additionally, the Tukey test was used for multiple comparisons.

Cloning | pARL15-myc was constructed using the PCR product of ARL15's coding sequence amplified from the template pARL15-GFP, with primers containing the myc tag sequence and AgeI and BamHI restriction sites (Primers A1 and A2). Then, the construct was digested with AgeI and BamHI and inserted in a pEGFP-C1 (Invitrogen©) plasmid lacking the GFP tag. **pMitoRab11aWT** was cloned by removing TOM20 mitochondrial sorting signal from pMitoCherry with AgeI and NheI restriction enzymes and fusing this sequence to the N-terminus of Cherry-Rab11aWT in plasmid pCherryRab11aWT, upon digestion with the mentioned enzymes. **pARL15-myc-mito** was cloned in two steps: first, the Bcl-2 C-terminus mitochondrial sorting signal was amplified with PrimerC1 and C2 containing BamHI restriction sites in both ends from HeLa genomic DNA. Second, the amplicon was digested with BamHI and fused to the C-terminus of the myc tag of the plasmid pARL15myc.

Upon vector ligation, plasmids were used to transform *E. coli* TOP10 by heat-shock. Bacteria were plated in plates with agarose-LB media supplemented with antibiotic specific to the plasmid and incubated at 37^0C. Clones were screened for the presence of the insert by PCR and restriction digestions. Positive clones were purified using with NZYminiprep kit and then sequenced to confirm sequence integrity.

CHAPTER 3 | Results

3.1. Validation of ARL15 as a host factor involved in IAV infection

IAV genome encodes a modest number of proteins that are insufficient to sustain its replication without using host resources. It is therefore not surprising that viruses take advantage of many host cellular pathways and machinery during infection. In particular, the small GTPase Rab11 was shown to have a prominent role in IAV infection, transporting the viral genome to sites of assembly, and directly influencing viral production[70,131–133]. Besides Rab11, recycling is regulated by several other factors that ensure vesicle biogenesis, cargo loading, movement, vesicle delivery and fusion with precise membranes. Such accuracy is ensured by networks of regulatory, effector, motor, membrane tethering and fusogenic proteins that remain unidentified for the transport of IAV genome. ARFs have been described to have important roles in the secretory pathway, having mostly been defined as operating at the level of vesicle biogenesis, although recently additional roles have been described. Hence, the goal of this project is to identify proteins from the ARF-family that are involved in the genome trafficking step.

3.1.1 Preliminary data: screening of proteins from the ARF-family required for vRNP trafficking during IAV infection

To identify ARFs involved in IAV infection, an immunofluorescence-based screen was carried out by B Kellen prior to my arrival at the lab. It aimed to identify interactions between ARF proteins and vesicles carrying the viral genome via quantifying the areas in which these proteins occupied the same cellular space. Determining co-localization between ARFs and vRNP-Rab11 vesicles presented several challenges due to: 1) low endogenous levels of ARF-family proteins in cells, 2) limited number of available antibodies for their specific labelling and 3) fast turn-over of vesicular membranal contents, with short lived interactions between Rab11 and ARFs. To mitigate these problems, GFP-tagged ARFs were overexpressed in cells treated with a drug previously shown to aggregate vRNP-Rab11 vesicles[73], that was used to enrich vesicular content. This drug,

known as nucleozin, was first described by Kao and colleagues[72], to display affinity for several domains of the viral protein NP even when this protein is coating viral RNA in vRNPs. At late times of infection, vRNPs are exported from the nucleus and are mostly attached outwardly to Rab11 vesicles. Here, nucleozin supplementation leads to vesicular "stapling" upon normal collision events that occur during transport, inducing the formation of dramatic cytoplasmic aggregates (figure 1.8b and 3.1b, middle panel).

The screen was prepared as follows: GFP-tagged versions of ARF-family proteins were transfected individually to infected cells. We considered the following small GTPases: ARFs (1, 3, 4, 5 and 6), ARLs (1, 2, 3, 4A, 4C, 4D, 5A, 5B, 8A, 8B, 9, 10, 13B, 14, 15, 16 and 17), ARF-related protein 1 (ARFRP1), Secretion-Associated Ras proteins 1A and B (Sar1A and Sar1B) and tripartite motif-containing protein 23 (Trim23). At 6 hours post-infection the drug nucleozin was added to induce aggregate formation, and increase spatial co-localization of the proteins with vRNPs. Infection was stopped at 8 hours p.i. by cell fixation with PFA.

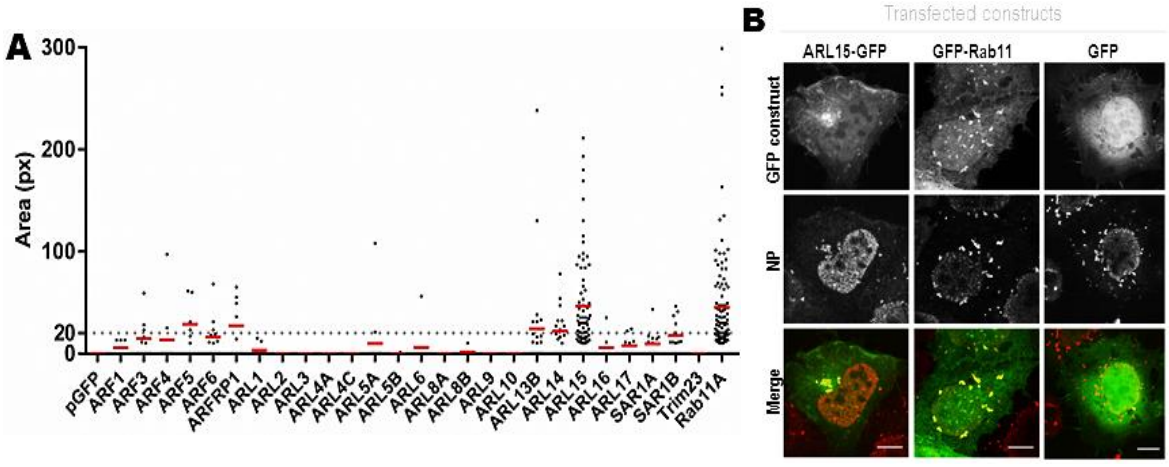

Figure 3.1. Role of ARF and ARL proteins in the biogenesis of vRNP-carrying vesicles. Screen of 26 GFP-tagged proteins of the ARF family: ARFs (1, 3, 4, 5 and 6), ARFRP1, ARLs (1, 2, 3, 4A, 4C, 4D, 5A, 5B, 8A, 8B, 9, 10, 13B, 14, 15, 16 and 17), Sar1 (A and B) and TRIM23 individually transfected in PR8-infected cells treated with nucleozin. At 8 hours p. i. cells were fixed and stained for viral protein NP. **a)** Individual overlapping areas between NP and each protein were sum and plotted as one dot per cell for comparison to the positive control Rab11-GFP (in pixel units). Co-localization between GFP and NP staining was assessed with ImageJ co-localization plugin. Red line in each column is the mean value of scores per candidate protein. The gray dotted line indicates the 20 pixel threshold. **b)** Representative images of cells transfected with ARL15-GFP (left panel), Rab11-GFP (middle panel) and GFP (right panel), infected with PR8 and treated with nucleozin from 6-8 h p.i.. At this time, cells were fixed and stained for NP protein (in red, middle panel) and imaged using the confocal microscope Leica Sp5. Scale bars represent 10µm.

To quantify the co-localization of each ARF protein with vRNPs, we scored the area of pixels overlapping between GFP and NP staining in absence and presence of

nucleozin. Without nucleozin, no candidate protein was observed to co-localize with vRNPs (data not shown). In the presence of nucleozin, the sum of the overlapping areas per cell was plotted as individual dots in figure 3.1a. As expected, the area of colocalization of viral protein NP and Rab11 was the highest score (mean of 45.69 pixels), and hence was used as positive control. Most ARFs tested gave modest values of co-localization, comparable to those obtained for the negative control GFP and NP (mean of 0 px). However, ARF5, ARFRP1, ARL13b ARL14b and ARL15 produced values higher than the 20 pixel threshold (means of 22.38, 21.75, 24.38, 22.06 and 45.65 pixels, respectively), being therefore good candidates to study further, as regulators of vRNP traffic. The most promising among the candidates was ARL15, with the highest score that resembled that of Rab11. For this reason, the role of ARL15 in IAV infection was further characterized.

3.1.2. Validation of the Screen

3.1.2.1 Effects of depleting endogenous ARL15 in IAV production using A549 cells

To validate the immunofluorescence-based screen, we made use of specific siRNAs for ARL15 (siARL15), or a control non-targeting RNA (siNT), to evaluate the effect of ARL15 depletion in viral production. For this purpose, three sequences that targeted endogenous ARL15 in the 3' untranslated region (3'UTR) were assessed in their ability to efficiently deplete ARL15. Thus, lung alveolar A549 cells were transfected individually with siRNAs targeting endogenous ARL15 (siARL15-1, -2 or -3), or with a combination of the three siRNAs in a mix, and with the control siNT for 36h (figure 3.2a). Afterwards, cells were infected at a MOI of 5 and at 16h p.i. supernatants were collected to quantify viral titers by plaque assays and cells were harvested for western blotting.

siARL15 depletion efficiency was confirmed by western blot. As observed in figure 3.2b, all siARL15 conditions efficiently reduced the levels of ARL15 in relation to the loading control GAPDH, in comparison to siNT. The levels of NP were used as a rough measure of the progression of infection in depleted *vs* non-depleted cells. As expected, uninfected cells did not express NP, whereas all conditions examined showed similar levels of NP in infected cells. This suggests that ARL15 does not influence early steps of the viral lifecycle, namely the entry stage and expression of viral proteins although further experiments should be performed to validate this assumption. The quantification of viral

titers (figure 3.2c) demonstrates that the knockdown of ARL15 led to a statistically significant reduction of viral production in all conditions. The most pronounced effect observed was obtained with siRNA-3 (15% ±7.5), although not statistically different to those of siARL15-1,2,3 (33% ±4.5) , siARL15-1 or -2 treatments (34% ±7.5, 35% ±1.0, respectively). From this point onwards, a mix of siARL15-1,2,3 was used whenever knockdown of endogenous ARL15 was required.

Hence, this assay successfully demonstrated that depletion of endogenous ARL15 affected viral production, reinforcing the outcome of the preliminary screen.

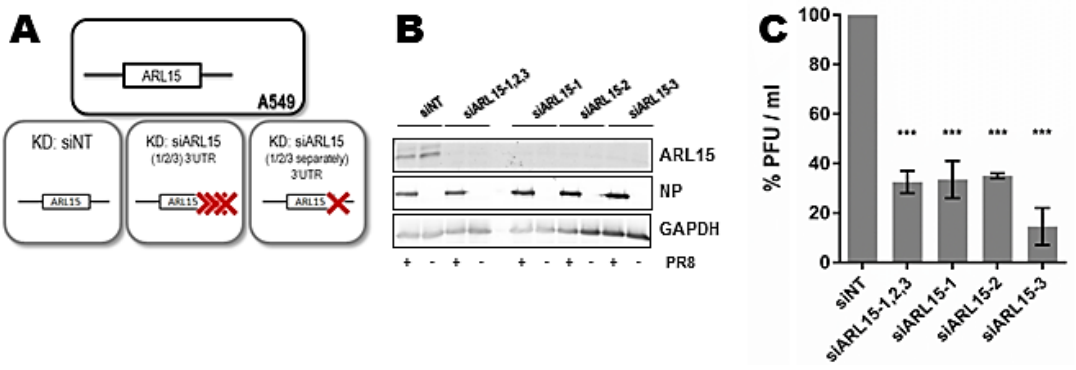

Figure 3.2. ARL15 depletion in A549 cell line. A) Strategy for ARL15 depletion. The following conditions were tested to deplete endogenous ARL15: non-targeting siRNA (siNT) as control; three individual siRNA targeting ARL15 3'UTR and a mix constituted of three siARL15 targeting 3'UTR of ARL15. (siARL15-1, -2, and -3). Upon depletion, cells were infected with PR8 at a MOI of 5, being harvested at 16 h p.i.: **b)** ARL15, the viral protein NP and the loading control GAPDH were analyzed by western blotting, and **c)** supernatants were collected and virus titers measured by plaque assays. The mean of virus titers from two experiments were normalized to siNT control and plotted as percentage of plaque forming units per milliliter. One Way ANOVA test was performed, with 95% confidence. (***) P<0.001.

3.1.2.2. Effects of depleting and rescuing ARL15 in IAV production using the ARL15-GFP stable cell line

The lack of specificity in siRNA treatments, on account of off-target activity, has been well documented[134,135]. Therefore, rescue experiments were planned to confirm the requirement of ARL15 in infection, in which, upon gene silencing, cells would be transfected with the coding region of the targeted DNA to revert the observed effect.

For this purpose, A549 stable cell lines were created expressing the GFP-tagged ARL15 used in the original screen. The presence of an endogenous sequence and a tagged construct coding for ARL15 enabled targeting independently these proteins by using siRNAs specific for different regions in the transcripts. Since ARL15-GFP plasmid lacks a 3'UTR, siRNAs targeting endogenous ARL15 3' UTR would not affect ARL15-GFP.

In turn, ARL15-GFP would be depleted by siRNAs targeting the fluorescent tag. As a control, A549 stable cell lines expressing 'GFP' were included in assays. The cells were established by S Costa and A Seixas prior to the beginning of this master thesis. GFP and ARL15-GFP stable cell lines were passaged presenting similar growth rates and expected intracellular localization of the GFP protein expressed (Fig 3.3a and b). Furthermore, cells were equally permissive to infection, producing similar viral titers (figure 3.3c). Given the similarities presented by the two cell lines, and to limit the sampling size of each experiment, only the ARL15-GFP stable cell line was used for the subsequent assays.

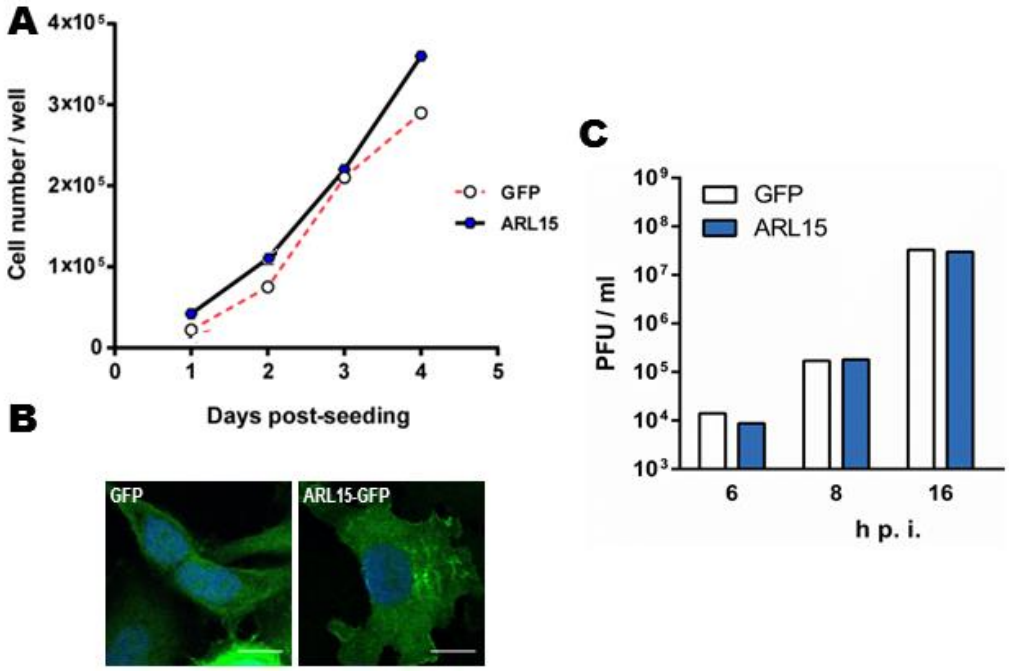

Figure 3.3. Characterization of A549 stable cell lines expressing GFP and ARL15-GFP. Cell lines were established using LentiORF pLEX-MCS Vector system (Thermo Scientific) according to manufacturer's instructions. Stable cell lines expressing GFP and ARL15-GFP were characterized for **a)** growth rates independently of viral infection, **b)** intracellular distribution of proteins (scale bars of 10µm) and **c)** viral production at 6, 8, and 16h p.i. upon PR8 infection at a MOI of 1.

To perform rescue experiments, I have used the ARL15-GFP stable cell line to deplete: 1) GFP, or 2) endogenous ARL15, or 3) the two proteins combined (figure 3.4a). For this purpose, cells were transfected with different combinations of siRNAs: either with a GFP-targeting sequence (siGFP), siARL15, a mix containing siGFP and siARL15, and siNT as control, and were incubated for 36h. After this time, cells were infected at a MOI of 5 for 16h, time at which supernatants and cells were harvested to perform plaque assays and western blots, respectively.

As above, depletion efficiency was confirmed by western blotting performed on cell lysates (figure 3.4b). Reduction in the levels of endogenous and overexpressed ARL15 was observed upon silencing (siARL15 and/or siGFP) when compared to the siNT control. Regardless of infection siGFP depleted ARL15-GFP but not ARL15 (figure 3.4b, lanes 3 and 4). Conversely, siARL15 only targeted ARL15 and not ARL15-GFP (lanes 5 and 6). siGFP and siARL15 efficiently blocked production of both ARL15 forms (lanes 7 and 8). Infection rate, as measured by NP staining, was invariable in all the conditions tested, when compared to the control. As in section 3.1.2.1, virus titers, normalized to control siNT, were reduced 10-fold (11%±2 PFU/mL) when siARL15 was transfected (figure 3.4c). Surprisingly, simultaneous silencing of endogenous and overexpressed ARL15 did not produce an exacerbation in the phenotype, as predicted. Rather, the levels of released virions were similar to those of siARL15 alone (15%±6 PFU/mL). However, targeting ARL15-GFP individually, resulted in an increase in viral titers (156% ±43), suggesting a role for ARL15-GFP in IAV inconsistent with the endogenous form.

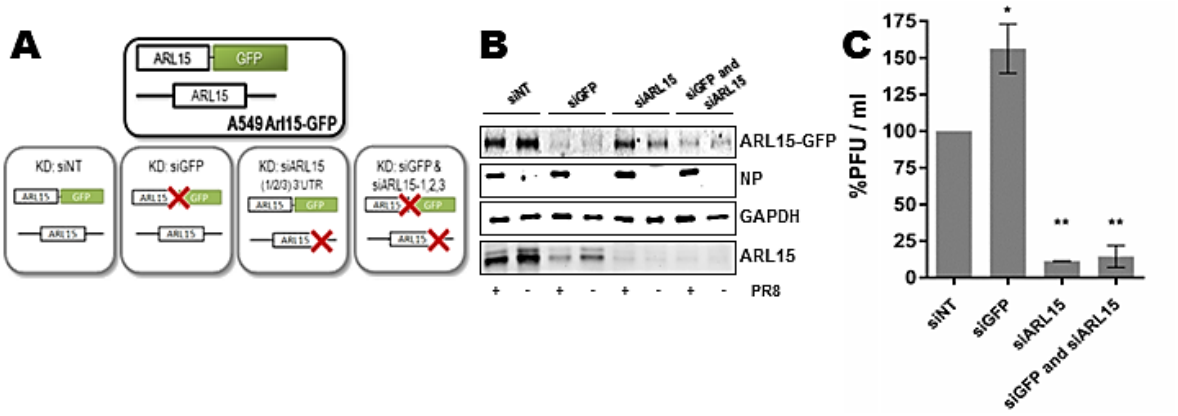

Figure 3.4. ARL15 depletion in A549 stable cell lines. a) Strategy of depletion: a non-targeting siRNA (siNT) was used as control; GFP-targeting siGFP was transfected for ARL15-GFP depletion and siARL15 was used for the *knock down* of endogenous ARL15. The latter two siRNAs were combined to deplete the overexpressed and the endogenous forms of ARL15. Cells were infected after 36 h of incubation, with an MOI of 5. At 16h p.i. **b)** cells were harvested for western blot. Approximately 10 000 cells ran in a 12.5% acrylamide gel, transferred to a nitrocellulose membrane and stained against GFP (ARL15-GFP), NP, Glyceraldehyde 3-phosphate dehydrogenase protein (GAPDH) and endogenous ARL15.**c)** supernantants were collected and virus titers normalized to siNT control. One Way ANOVA test was performed, with confidence of 95%. (*) P<0.05; (**) P<0.01.Graphs include values obtained in two independent experiments.

This assay suggested that either ARL15-GFP was not catalytically functional, or that siRNAs targeting the endogenous form of the protein were having off target effects, affecting other transcripts that influenced IAV infection.

3.1.2.3. Rescue of viral production with ARL15-myc and ARL15-GFP constructs

To distinguish between the two hypotheses: non-functional ARL15-GFP or off-target effects of the siARL15, complementary rescue experiments were performed using a new ARL15 plasmid cloned with a different tag. For this purpose, the coding sequence of ARL15 was fused to a tag containing 10 aminoacids (myc tag) instead of the 238 aminoacids that constitute the GFP tag.

Rescue experiments were performed to test, in parallel, the ability of ARL15-GFP and ARL15-myc to revert the effects of siARL15 on viral production. Notably, neither construct is susceptible to siARL15 as they lack the 3'UTR. For consistency, each sample was transfected with a siRNA and a plasmid as detailed in figure 3.5a. As controls, we transfected HEK 293T cells with the pGFP plasmid and the siNT siRNA. This condition was then compared to the following transfections: siARL15 with pGFP; siARL15 with pARL15-myc and siARL15 with pARL15-GFP. Of note, HEK 293T cells were used to ensure high transfection rates. Upon co-transfection with siRNAs and plasmids for 36 hours, cells were infected with PR8 at a MOI of 5. Supernatants were harvested at 16 hours p.i. for plaque assays and cells for western blotting to assess viral titers and viral protein expression, respectively.

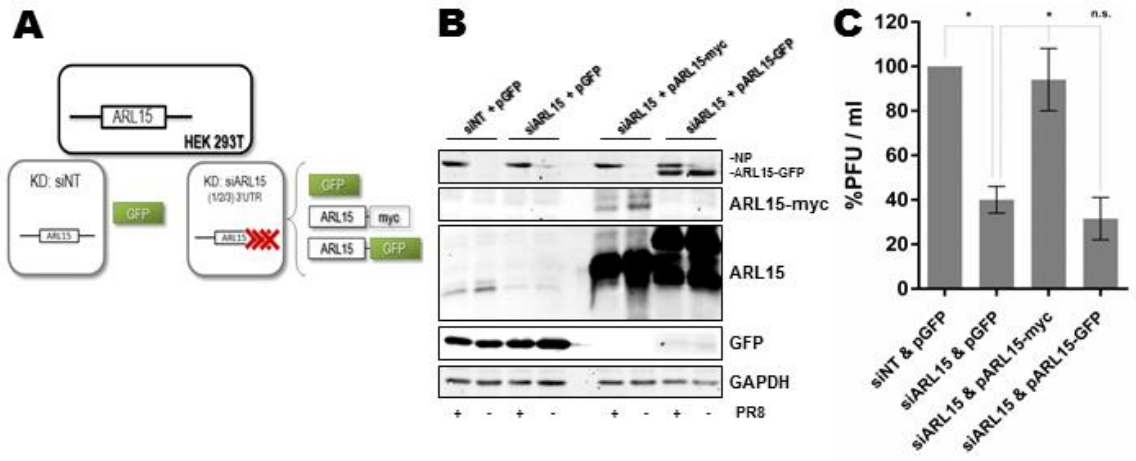

Figure 3.5. Rescue assay in HEK 293T cells. a) Strategy of transfection for the rescue assays. The following conditions were used: a control condition with non-targeting siRNA (siNT) and overexpression of pGFP; siARL15 and pGFP; siARL15 and pARL15-myc, and siARL15 and pARL15-GFP. After 36 h incubation, cells were infected and mock infected and incubated for further 16h before assessing **b)** Viral and host cell expression by western blot of approximately 10 000 cells that were stained for NP, GFP, Myc, and GAPDH. **c)** Virus titers were normalized as percentage of the condition siNT & pGFP control. One Way ANOVA test was performed, with confidence of 95%. (*) $P<0.05$; (n.s.) non-significant. Experiments are representative of two independent repeats.

Immunoblotting of cell lysates (figure 3.5b) confirmed that cells expressed the indicated transfected constructs and that NP levels, a measure of infection rate, were fairly constant in all the conditions, in comparison to the loading control GAPDH.

Figure 3.5c shows viral titers of all conditions as a percentage of the control siNT & pGFP. Consistent with previous assays, the depletion of ARL15 showed significantly decreased viral titers with pGFP overexpression (40% ±6). When depleted cells were supplemented with ARL15-GFP, viral titers remained similar to the previous condition, which is consistent with results of section 3.1.1, shown in figure 3.4c. However, pARL15-myc transfection successfully rescued viral production to control levels (94% ±14 PFU/mL), which confirms the role of ARL15 in IAV infection.

This assay strongly suggested that the tag added to the C-terminus of ARL15 somehow influenced its functionality. While the original screen assay, performed with the non-functional ARL15-GFP, resulted in co-localization of vRNPs and ARL15 in nucleozin-induced aggregates, it is unclear whether this result would be observed with the ARL15-myc plasmid. Therefore, in the following section, the presence of ARL15-myc in nucleozin-induced vRNP aggregates will be assessed.

3.1.3. ARL15-myc localization in infected cells treated with nucleozin

With the intent of recapitulating the screen presented as preliminary data, the presence of ARL15 was analyzed by immunofluorescence in vRNP aggregates induced by nucleozin treatment. Several attempts were required to perform this simple experiment. At first, we tried to use commercially available antibodies against the endogenous ARL15, but the protein was not detected by immunofluorescence. To overcome this, the functional ARL15-myc was supplied exogenously to cells that were subsequently co-infected as in the original screen. However, the anti-myc antibody used in immunofluorescence did not detect any specific staining of ARL15-myc, suggesting that the tag was hidden once fused to ARL15. Finally, and upon several rounds of troubleshooting assays (data not shown), it was found that the antibody against ARL15 efficiently stained ARL15-myc. Thus, HeLa cells were transfected with the plasmid pARL15-myc for 16 hours and infected with PR8 at a MOI of 10. Nucleozin was added to a set of duplicate samples two hours prior to fixation, which took place at 8 and 10 hours p.i.. Cells were then immunostained against NP and ARL15 and imaged by confocal microscopy.

In all infected conditions, ARL15-myc distribution consisted of cytoplasmic dispersed puncta, which lacked NP co-staining in cells without nucleozin (figure 3.6, 8h p.i.

and 10 h p.i. top lanes). As expected, in nucleozin-treated cells, NP distribution was altered from dispersed puncta, characteristic of vesicular transport, to large aggregates (figure 3.6, +Nz bottom lanes). These vRNP aggregates were however, devoid of ARL15 and therefore, the two proteins did not overlap. However, close examination of aggregates showed that ARL15 could be observed in their vicinity. The significance of this proximity, if any, is still unclear.

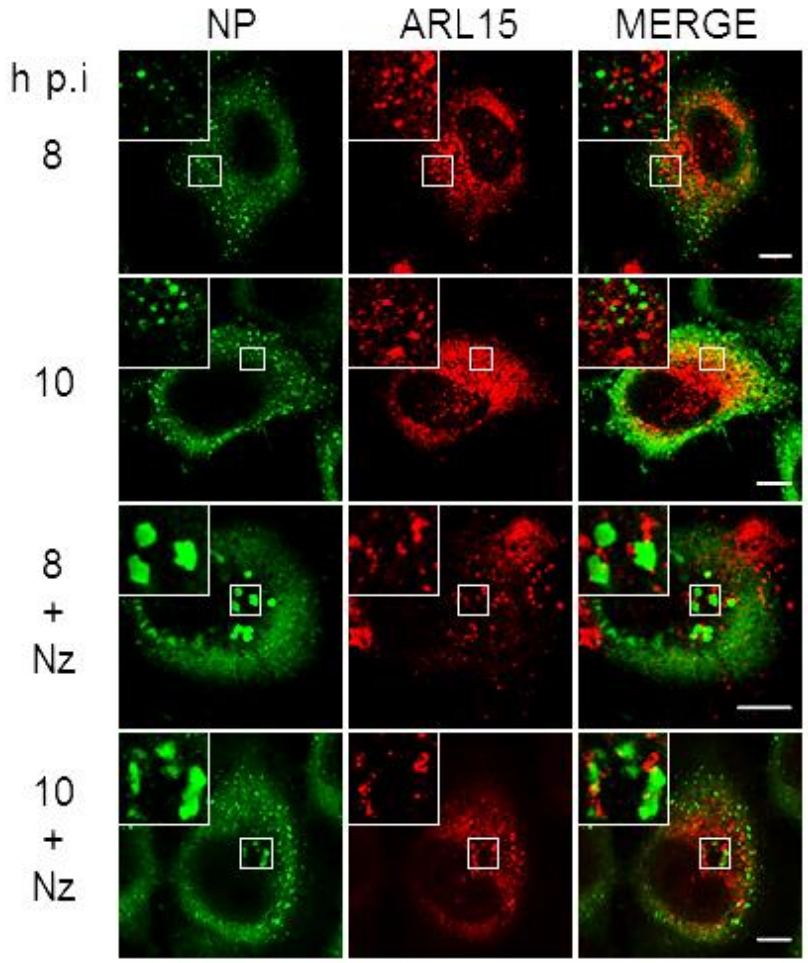

Figure 3.6. ARL15-myc is excluded from nucleozin-induced vRNP aggregates. HeLa cells transfected with pARL15-myc and infected at a MOI of 10. 2 hours prior to fixation, cells were treated or mock-treated with 2µM nucleozin and at 8 and 10 hours post-infection cells were fixed. Samples were stained for ARL15 and viral protein NP. Images were acquired by confocal microscopy. Scale bars of 10µm.

Hence, this assay did not recapitulate the initial screen that positively identified ARL15-GFP in vRNP-Rab11 vesicles. The most obvious difference between assays is the tag used in ARL15 plasmids, which could be the cause underlying the different outcomes. This hypothesis is in agreement with ARL15-GFP failure to rescue viral production in the

siRNA experiment, in contrast to the ARL15-myc version. In fact, these results allow the speculation that ARL15-GFP folded into a non-functional arrangement, that is either catalytically inactive or in which the GFP tag might be concealing a domain in ARL15 that is important during traffic. Tempting as it may be, this hypothesis awaits confirmation.

Overall, the decreased viral production caused by the lack of ARL15, and the consistent rescue of this phenotype upon ARL15-myc overexpression, indicates that ARL15 plays a role during IAV infection that remains uncharacterized and will be the focus of the next chapter.

3.2. Characterization of ARL15 function during IAV infection

3.2.1. Introduction on ARL15

ARL15 function is unknown, although its predicted amino acid sequence suggests that it is structurally linked to ARFs (and Ras-related GTP binding proteins), which play key roles in regulating trafficking. Literature is limited to associations of ARL15 polymorphisms with diabetes[136,137] and other diseases such as rheumatoid arthritis[138], identified by genome wide screens. Generally, ARL15 is a conserved protein[116], ubiquitously expressed in chordates and absent in lower eukaryotes. Figure S1, in supplementary data, shows the homology tree of the alignment between ARL15 sequences from humans, apes, mice, chickens, frogs, among others, with overall 63% identity. The remaining characterization of ARL15 is based on the predicted amino acid sequence. Thus, ARL15 is expected to be intracellular[139], although it has also been identified extracellularly[140], namely in exosomes isolated from urine[141,142] and secretions of ovarian[143] or prostatic[144,145] cells.

On a structural level, ARL15 characterization is based on sequence alignment for identifying functional domains. These include a GTPase region and a P-loop domain with a conserved nucleotide phosphate-binding motif – both characteristics are shared among ARFs (figure S2 in supplementary data). The homology tree in figure S3 was based on sequences retrieved from Uniprot database and show the SAR1 isoforms, SAR1a and SAR1b, as the closest members to ARL15. Alignments of the three peptides are depicted in figure S4, where algorithms predicted GTP and Mg^{2+} binding domains and 'switch' regions in ARL15 by comparison with SAR1. Finally, attachment of ARL15 to membranes might involve palmitoylation at the N-terminus on well-conserved cysteines[116], instead of the typical myristoylation modification observed in the remainder ARFs.

Overall, ARL15 is vastly uncharacterized and potentially involved in important human diseases that have been linked to trafficking defects[146]. The addition of a pathogen to this list, such as IAV, suggests that its role in regulating the secretory pathway might be more prominent than anticipated and argues in favor of studying its function.

3.2.2. Quantification of total ARL15 during infection

In order to observe if ARL15 expression was altered during infection with PR8, cell lysates were collected over a time course and processed for western blotting. For this purpose, A549 cells were infected at a MOI of 5 with PR8, harvested at 4, 8, 12, 14, 16 and 18h p.i. and stained for NP, ARL15 and GAPDH, as a way to assess infection, ARL15 expression and control for sample loading. As expected, NP levels increased during the course of infection. Conversely, ARL15 was unaltered during infection (figure 3.7), presenting similar levels to those found in mock-infected cells. Furthermore, the maintenance of ARL15 levels throughout infection seems to be a general characteristic of IAV infection as similar results were obtained with infection of other viral strains such as X31 (H3N2) and MUd (H1N1), see figure S5 in supplementary data.

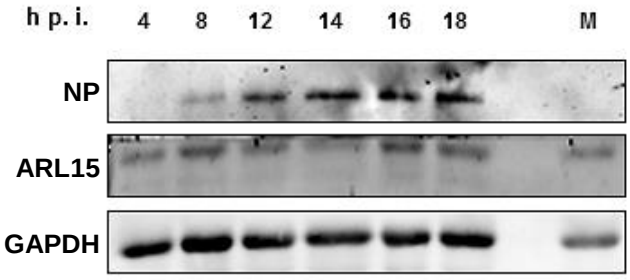

Figure 3.7. ARL15 levels during infection determined by western blot. A549 cells were infected at a MOI of 5 with PR8, and harvested at 4, 8, 12, 14, 16 and 18h p.i.. Cell lysates were run in a 15% acrylamide gel, transferred to a nitrocellulose membrane and stained for NP, ARL15 and GAPDH.

Upon assessing the total levels of ARL15, we studied its intracellular distribution. The subcellular localization of most ARL proteins remains uncharacterized. However, these are expected to cycle between the cytosol and specific membranous compartments, depending on their activation status. ARFs when switched-off bind GDP and are cytosolic, whilst the GTP-bound forms are switched-on and recruited to their target membrane[147], attracting effectors to execute its function. Therefore, viral-induced alterations in ARL15 might not be regulated at the level of expression but rather downstream at the level of activation. The latter may be related with changes in distribution and will be assessed in the following section.

3.2.3. Distribution of ARL15-myc during infection in HeLa cells

In order to observe ARL15 localization during infection, pARL15-myc was overexpressed in HeLa cells (due to the antibody limitations previously described). Upon transfection for 16 hours, cells were infected at a MOI of 10 and fixed at 2, 4, 6, 8 and 10h p.i.. Samples from the last time points were, in addition, incubated with nucleozin two hours prior to fixation. Cells were then immunostained against ARL15, NP and the Golgi Brefeldin-A resistant guanine nucleotide exchange Factor 1 (GBF1), present at the cis-Golgi and analyzed by confocal microscopy (figure 3.8a).

In mock infected cells, ARL15 showed perinuclear accumulation consistent with the cis-Golgi that was marked by the host protein GBF1. In addition, ARL15 was found diffused within the cytoplasm, with increased concentration at the extremities, highlighting cellular edges and projections. Upon infection, the distribution of ARL15 was altered in two different ways. First, the overlap between ARL15 and GBF1 staining was progressively lost (figure 3.8a, right-side zoomed panel). These differences were quantified using Pearson Correlation Coefficient that decreased significantly during infection (figure 3.8b). Second, the presence of ARL15 at the extremities of cells also diminished, and cellular projections were no longer evident. These results indicate that ARL15 might leave the cis-Golgi and cellular extremities, as soon as infection begins, remaining at an unknown subcellular compartment.

Given that ARL15-myc and the ARL15-GFP constructs showed different abilities to rescue ARL15 depletion, the cellular distribution of ARL15-GFP was also examined. Our rationale was to identify if the changes in distribution of ARL15 would be required for its function in infection. This experiment was performed using the ARL15-GFP stable cell line, whose construct was unable to rescue depletion of endogenous ARL15.

Throughout infection, ARL15-GFP did not show differences in localization when compared to mock infected cells (figure S6 in supplementary data). It exhibited a cytoplasmic punctate distribution, accumulating at the cellular extremities and in a perinuclear compartment (possibly the cis-Golgi), and surprisingly it also stained the nucleoli. Providing that this construct might not be functional, the relevance of this distribution is unclear.

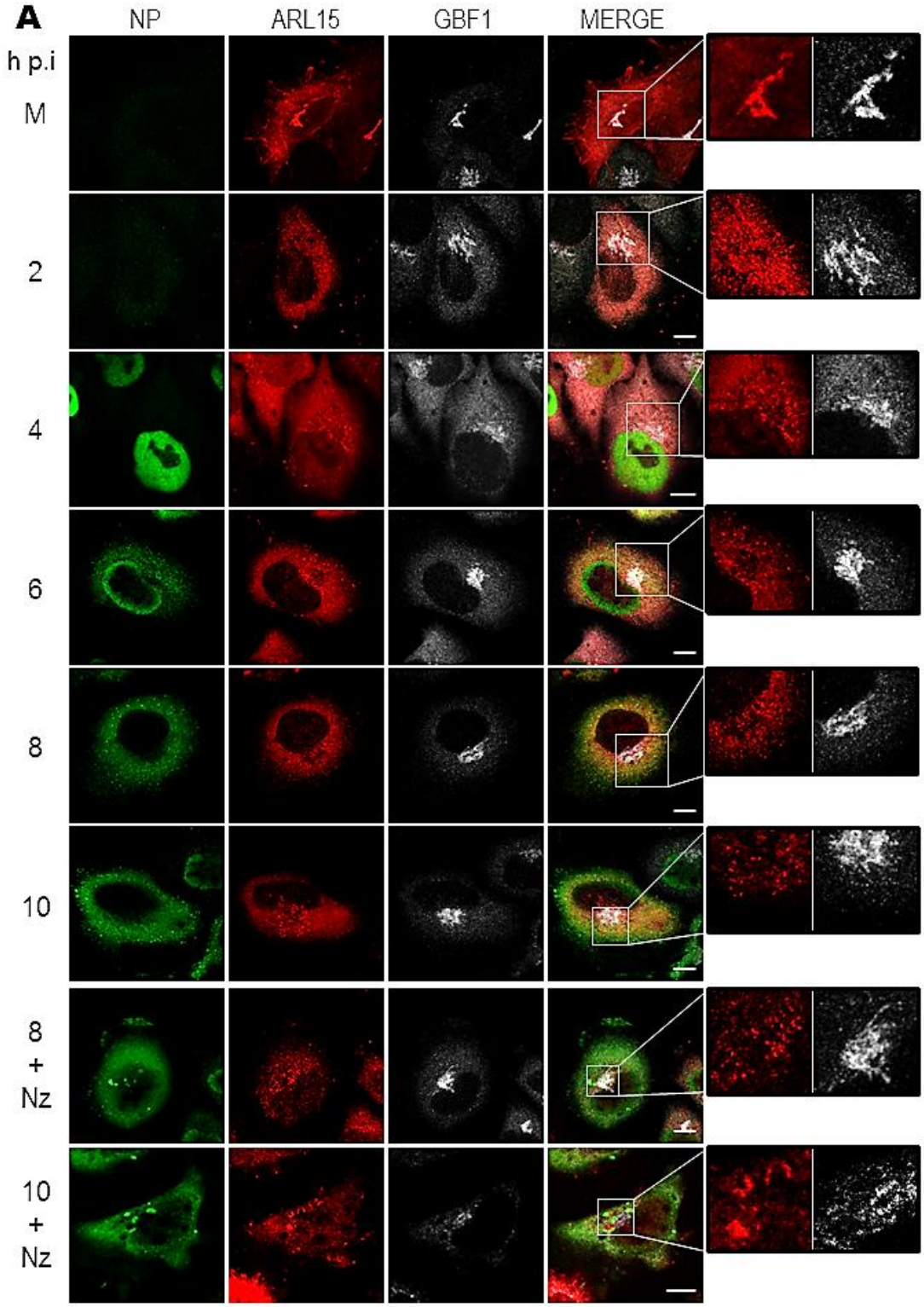

Figure 3.8. ARL15-myc distribution during IAV infection. (continues in the next page)

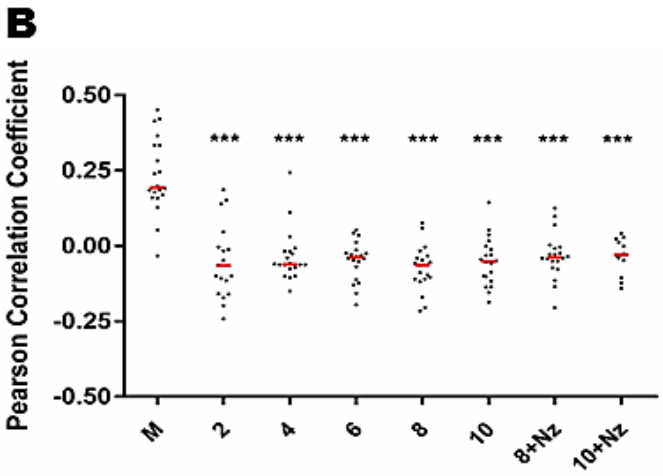

Figure 3.8. ARL15-myc distribution during IAV infection. a) HeLa cells were transfected with pARL15-myc and infected at a MOI of 10. Cells were fixed with 4% PFA at 2h, 4h, 6h, 8h, 10 h p.i. and stained for ARL15 (in red), the viral protein NP (in green) and GBF1 (in grey). In nucleozin treated cells, 2µM of the drug was added two hours prior to fixation. Images acquired by confocal microscopy. Error bars are of 10µm, except when mentioned. **b)** Pearson correlation coefficient for co-localization between ARL15 and GBF1. 20 cells analysed per condition. One Way A-Nova test was performed, with confidence of 95%. (***) P<0.001. Assay and measurments performed once.

Thus, these results suggest that the myc-tagged ARL15 changed its localization upon infection, whilst the GFP form did not. This observation corroborates that these constructs are indeed distinct, but additionally suggests that ARL15 needs to undergo an unknown alteration to positively influence viral infection, by an unknown mechanism that we aim to understand. The close proximity between ARL15 and cytoplasmic vRNPs and our preliminary screen argue in favor of assessing the role of ARL15 in promoting vRNP transport.

3.2.4. vRNP distribution upon ARL15 depletion in A549 and ARL15-GFP stable cell lines

To understand whether ARL15 was involved in vRNP trafficking, the strategy was to visualize the effects of depleting ARL15 in vRNP transport, using the above characterized siRNAs in both A549 cells and the ARL15-GFP stable cell line, the latter used as a control. Since the change in ARL15 distribution occurred at early stages in infection, the protein could facilitate traffic of the viral genome to the nucleus upon viral entry. Alternatively, the close proximity of cytoplasmic vRNPs and ARL15 late in infection also suggest that ARL15 could play a role in late stages of infection, namely in the transport of vRNP or other viral proteins to the sites of viral assembly. Literature postulates

that upon vRNP loading onto Rab11-positive vesicles, vRNPs are found in punctate cytoplasmic structures[70,131–133], whose size increases during infection, as a result of impairment in recycling efficiency [Costa SV *et al* 2015, unpublished]. A failure in this loading process leads to a dispersed distribution of NP throughout the cytoplasm.

To this end, A549 or ARL15-GFP cells were transfected (in independent experiments) with siNT or siARL15. Additionally, the stable cell line was also treated with siGFP alone or in combination with siARL15. Upon transfection for 36h, cells were infected with PR8 at a MOI of 5 and fixed at 16 h p.i.. Then, cells were processed for immunofluorescence and stained for NP to be analyzed by confocal microscopy to assess trafficking of vRNPs. Figure 3.9 illustrates the depletion assays performed in A549 cells, and figure 3.10 in the ARL15-GFP stable cell line. The distribution of NP was found in punctate structures throughout the cytoplasm in both siRNA treatments in the two cell lines. This suggested that vRNPs were present in Rab11-positive vesicles with distribution characteristic of the recycling pathway, regardless of ARL15. However, the areas of vesicles of vRNPs seemed to be larger upon depletion of ARL15 in both cell lines tested. To quantify the area of NP vesicles, we used two strategies. The first was to plot the mean of the areas obtained per cell and the second was to separate vesicles into three arbitrary categories according to size: small vesicles ranged from 0 to 0.2 µm², intermediate size vesicles from 0.2 to 0.4 µm² and large with areas over 0.4 µm².

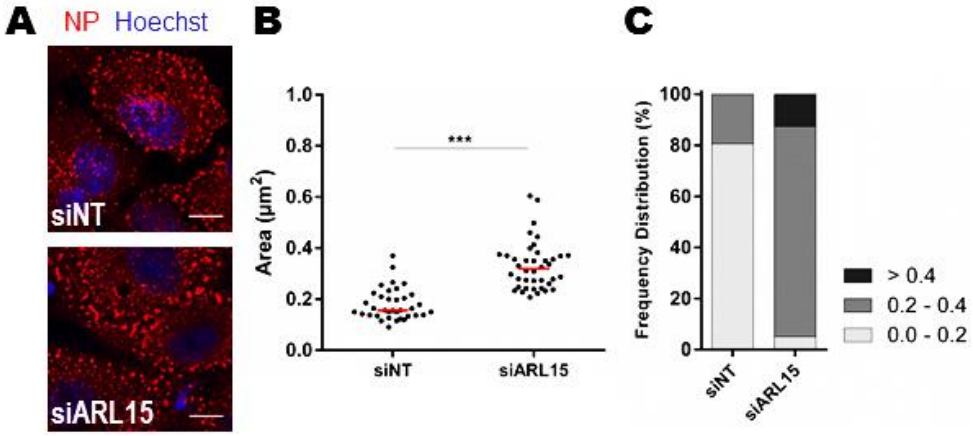

Figure 3.9. vRNP distribution upon ARL15 depletion in A549 cells. a) A549 cells transfected with either siNT or siARL15-1,2,3 for 36 hours, and infected at a MOI of 5. Cells were fixed at 16h p.i. in 4% PFA and immunostained against NP and Hoechst. Images were acquired by confocal microscopy. Scale bars represent 10µm. **b)** Vesicle size in each cell was measured using Fiji 'Analyse Particles' plugin. The mean value of all vesicles' area in a cell was represented by one dot plotted on the graph. Red line represents the median value. Student t-test was performed with confidence of 95%. (***) P<0.001. 35 cells were analysed per condition. **c)** Percentages of values plotted in b), distributed by ranges. Assay and measurements were performed only once and require repetition.

In A549 cells, vesicles carrying vRNPs duplicated in area when ARL15 was depleted, with median size of 0.32 µm², compared to the control siNT of 0.16 µm² (figures 3.9a and b). This result was corroborated by a 64% increase in vesicles of intermediate size upon siARL15 treatment, as observed in the frequency distribution plot (figure 3.9c). Furthermore, cells treated with siARL15, rarely showed NP at the cell periphery.

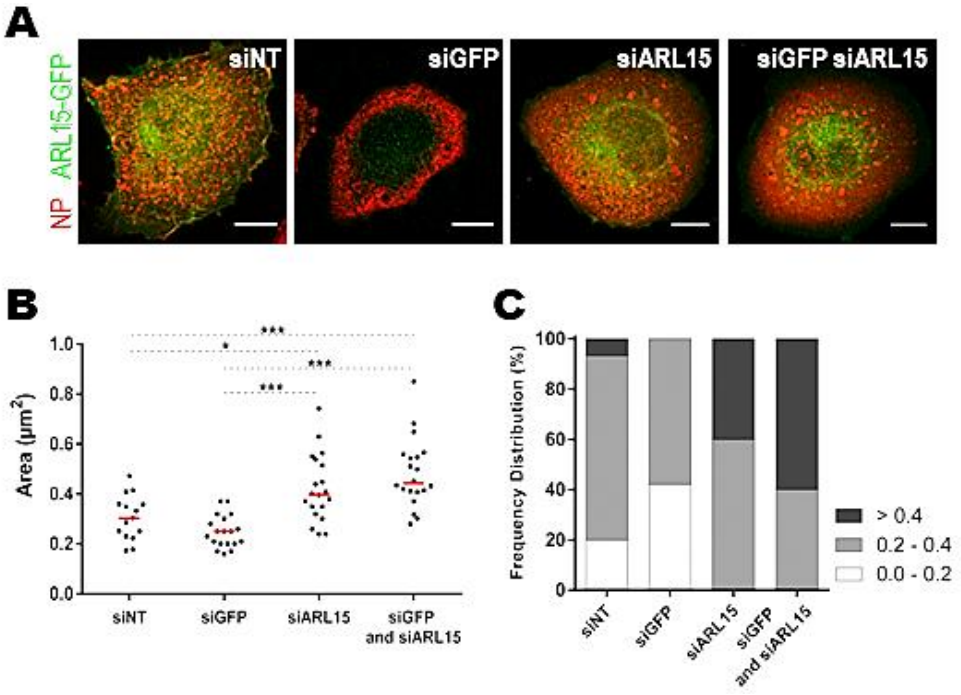

Figure 3.10. vRNP distribution upon ARL15 depletion in the ARL15-GFP stable cell line. a) A549 cells stably expressing ARL15-GFP were transfected for 36h with either siNT, siGFP, siARL15, or the latter two combined, and then infected at a MOI of 5. Upon fixation at 16h p.i., cells were immunostained against NP. Images were acquired by confocal microscopy. Scale bars represent 10µm. **b)** Vesicle area in each cell was measured using Fiji 'Analyse Particles' plugin, and the average plotted in a graph. Red line represents the median value. One Way ANOVA test was performed, with confidence of 95%. (*) P<0.05; (***) P<0.001. 20 cells were analysed per condition. **c)** Percentages of values plotted in b), distributed by ranges. Assay and measurements were performed only once and require repetition.

In the stable cell line, endogenous ARL15 depletion likewise resulted in increased vesicle size. Consistently, the median area of vesicles was of 0.40 µm² for siARL15 and 0.44 µm² for siARL15-siGFP conditions, when compared to control siNT whose vesicles showed a medium size of 0.30 µm². Moreover, the depletion of ARL15-GFP did not affect vesicle size, with median area of 0.26 µm² (figure 3.10a and b), which is also obtained in the frequency distribution plot (figure 3.10c). Although intermediate values remain constant in all transfections, the percentage in larger vesicles increased in siARL15 and siARL15/siGFP conditions by 30 and 60%, respectively. In addition, vRNPs were less

visible at the cell periphery, an observation that was facilitated by the GFP fluorescent background.

Overall, the knock down of endogenous ARL15 consistently resulted in enlarged vRNP-carrying vesicles. Such enlargement could reflect the underlying reason for the reduced viral titers observed upon ARL15 depletion, in section 3.1 of Results. ARL15 knock down seems to accumulate vRNPs in the cytoplasm, suggesting an impairment of vRNP transport towards the cellular periphery prior to budding out of the cell. Hence, we set up a strategy to observe if ARL15 would recruit vRNPs to Rab11 vesicles.

3.2.5. Recruitment of vRNPs to the mitochondria upon transfection of Mito-Rab11 and ARL15

The viral genome, in the form of vRNPs, is loaded onto Rab11-positive vesicles upon nuclear export and is transported using the microtubule network towards the plasma membrane. The enlargement of NP vesicles could be explained by two hypotheses: 1) ARL15 depletion could promote vRNP loading on Rab11 vesicles or 2) it could inhibit vRNP delivery to the plasma membrane. Our group has implemented a synthetic system for the study vRNP-Rab11 traffic, based on the targeting of Rab11 to a random organelle, the mitochondria. Data acquired by other lab members show that in the case of Rab11-WT being targeted to this arbitrary compartment, vRNPs follow in a reasonable percentage, also localizing to the mitochondria (figure S7, supplementary data). In principle, the effects of ARL15 in promoting Rab11-vRNP interaction or delivery of vRNPs to membranes could be indirectly assessed by quantifying vRNP-Rab11 mitochondrial overlap in the presence or absence of ARL15. To perform this quantification, two forms of Rab11 were included: the wild-type (WT) able to bind vRNPs when switched on, and a GDP-bound dominant negative (DN) mutant, unable to recruit vRNPs.

To perform this assay, HeLa cells were co-transfected with two sets of plasmids: 1) pARL15-myc or pGFP as control and 2) a mitochondria-targeted plasmid expressing either: mcherry alone as a control (pMito-cherry) or fused to Rab11-WT or -DN forms (pMitoRab11aWT and pMitoRab11aDN). Upon infection with PR8 at a MOI of 20, cells were fixed at 16 hours p.i., immunostained against NP and ARL15 and imaged by confocal microscopy. Co-localization between mitochondria-targeted constructs and NP staining

was assessed using Fiji 'Colocalization Finder' plugin, the Pearson's correlation coefficient was measured per cell and plotted in a graph.

The vRNP localization at the mitochondria produced mean negative scores for control MitoCherry and MitoRab11-DN constructs, verifying that these are unable to recruit the viral genome, independently of the addition of ARL15 (figure 3.11a and b). In case of MitoRab11-WT overexpression, vRNPs localized to the mitochondria when the positive control GFP was co-transfected, whereas it appeared more diffuse in the presence of ARL15-myc. Scores support the observed effect caused by ARL15 in vRNP distribution, having mean values of 0.23 and 0.06 for pGFP and pARL15-myc, respectively. Although indirect, these results indicated that ARL15 might contribute to vRNP unloading of Rab11. This premise associated with the evidence of ARL15 being a positive regulator of IAV infection suggests that such a step would occur late in infection.

Overall, the data herein presented supports a relevant role for ARL15 in facilitating vRNP traffic at late stages of IAV infection, with a role in disturbing the binding of vRNPs to Rab11.

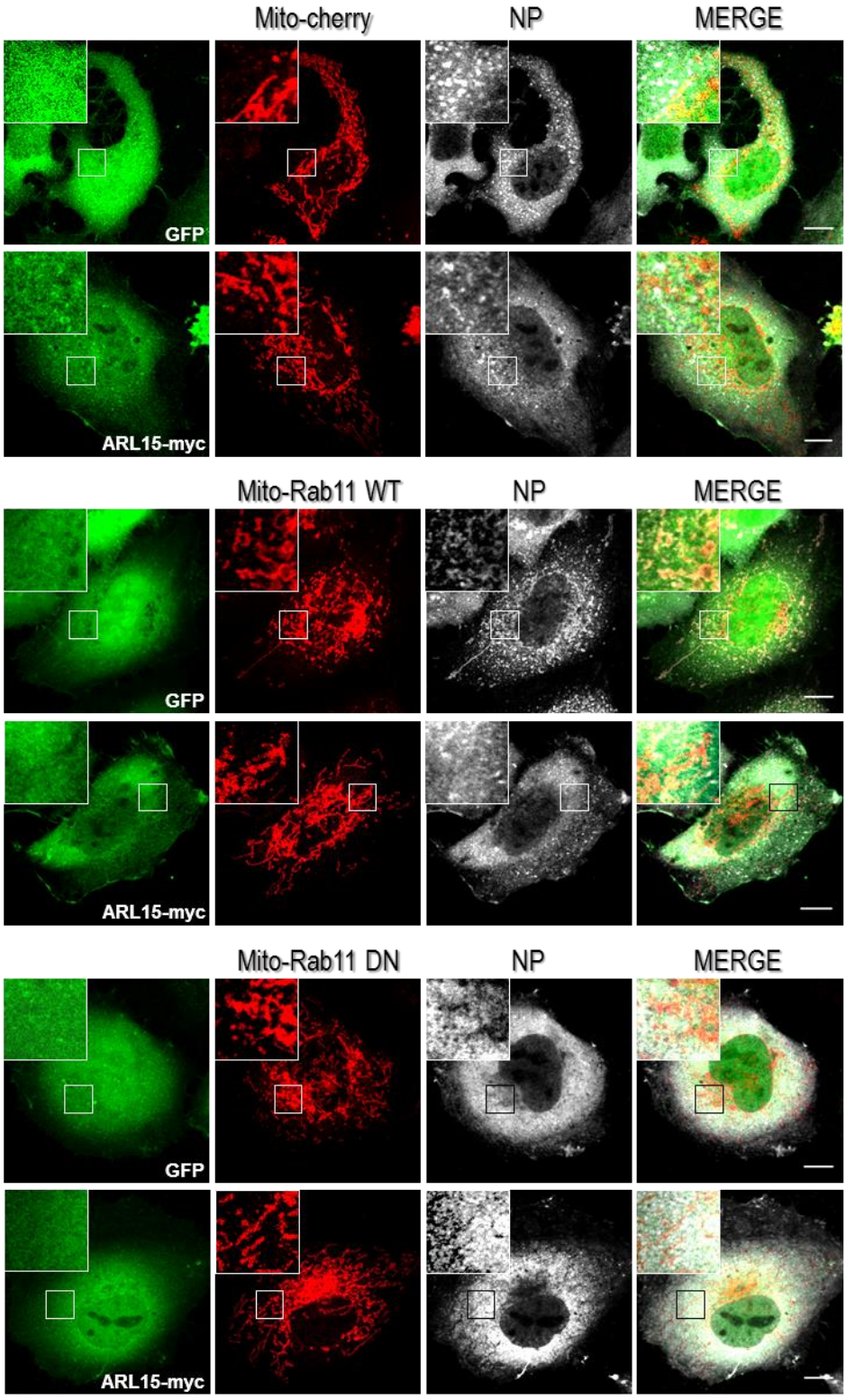

Figure 3.11. ARL15 affects the recruitment of vRNPs by Rab11. (continues in the next page)

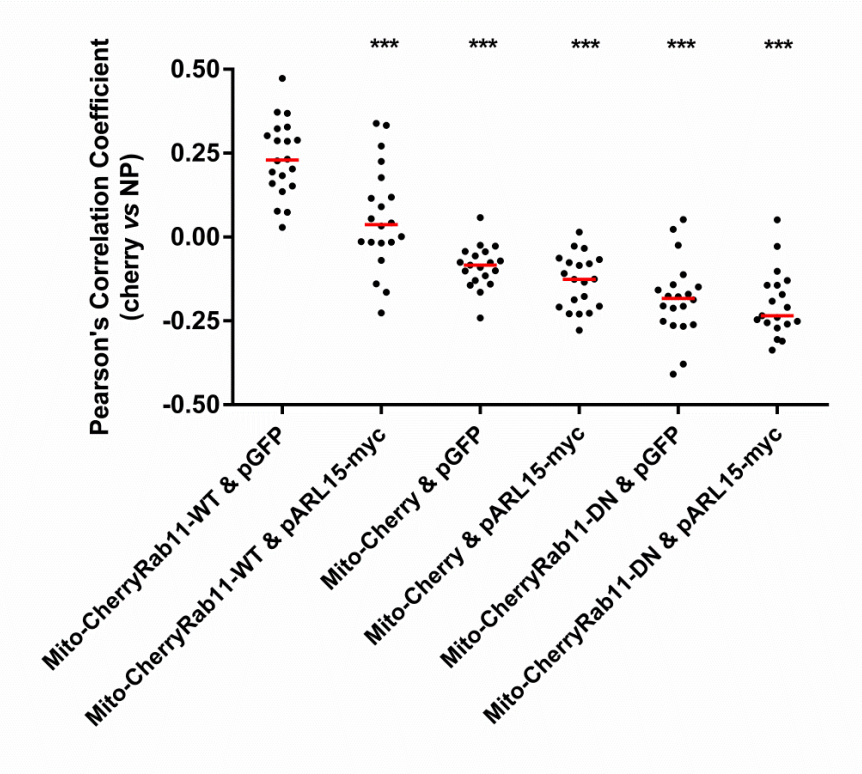

Figure 3.11. ARL15 affects the recruitment of vRNPs by Rab11. a) HeLa cells infected at a MOI of 20 and co-transfected with the following plasmid combinations: 1) Mitochondria targeted cherry (top panel), cherry-Rab11-WT (middle panel) or cherry-Rab11-DN (bottom panel) and 2) GFP or ARL15-myc. Cells were fixed in 4% PFA at 16h p.i. and stained for ARL15 and viral protein NP. Images acquired by confocal microscopy. Error bars of 10µm. **b)** Pearson correlation coefficient for co-localization between cherry-tagged construcs and NP. 20 cells were analysed per condition and One Way A-NOVA test was performed, with confidence of 95%. (***) P<0.001. Assay and measurments performed once.

CHAPTER 4 | Discussion

IAV is an important human pathogen that provokes frequent epidemics worldwide. Its infection is currently prevented by: vaccines that require constant updating on account of continually mutating viruses and antivirals, targeting NA, susceptible to select resistant strains. Novel antiviral strategies are needed and an alternative strategy could target key host pathways in sustaining viral replication. Recent findings revealed that IAV uses the recycling endosome for trafficking of the newly-synthesized viral genome, i.e. vRNPs. The major regulator of this compartment, Rab11, is known to bind progeny vRNPs, upon nuclear export. All segments that constitute the viral genome are loaded onto Rab11-positive vesicles and transported using the microtubule network towards the plasma membrane. It is likely that other host factors influence these processes, such as members of the ARF-family, since these, along with Rabs, control vesicular trafficking to ensure specific cargo delivery.

To determine the involvement of ARF-family members in IAV infection, we screened for the presence of these proteins overlapping with vRNP-carrying vesicles in an immunofluorescence based assay. For this purpose, GFP-tagged proteins were overexpressed in infected cells treated with nucleozin, a drug that specifically aggregates vRNP-Rab11 vesicles. The experiment provided a strong candidate, ARL15, which co-localized with NP aggregates in levels equivalent to those exhibited by Rab11. This ARL was never considered as a host factor required for IAV infection in genome wide screens[148–151], being very infrequently mentioned in literature. Nevertheless, it was identified as a genetic risk factor in diseases with marked trafficking defects such as diabetes and rheumatoid arthritis[136–138], and for all these reasons was the object of this thesis.

Depletion of the endogenous ARL15 decreased viral titers by 60-90% in all cell lines tested, suggesting that ARL15 has a positive role in the IAV lifecycle (see figures 3.2 and 3.4). However, the depletion of the exogenously supplied ARL15-GFP could not rescue viral production (figure 3.4), in the ARL15-GFP stable cell line. These conflicting results could be attributed to: 1) siRNA off-target effects on transcripts other than the

endogenous ARL15 or 2) impairment in ARL15 activity caused by the addition of the bulky GFP tag. To distinguish between the two scenarios, rescue assays were performed using a distinct plasmid encoding ARL15 fused to the myc-tag (figure 3.5). Remarkably, ARL15-myc, unlike ARL15-GFP, was able to rescue viral titers to control levels, indicating that ARL15 favored IAV infection and validating the screen herein presented as preliminary data. However, results also suggested that the GFP-tagged construct was somehow non-functional. The premise for the initial screen was to find functional ARF/ARLs in vRNP aggregates. Since ARL15-GFP was suggested to be non-functional, ARL15-myc distribution was assessed in enriched vesicular content of vRNPs and Rab11 induced by nucleozin, and found to be excluded from vRNP aggregates (figure 3.6). Close inspection of these aggregates showed that ARL15 was consistently found in their vicinity. Nevertheless, this result contrasts with the one obtained with the initial screen due to reasons that are unclear at this point. Still, the observed proximity between vRNP aggregates and ARL15, suggests that they might interact, although via an intermediate complex able to bridge ARL15 to an undefined component of vRNP-carrying vesicles. Such a mechanism resembles other cellular mechanisms described, for example, the ability of ARL8 to recruit the effector SKIP which attracts Kinesin-1 to control the distribution of lysosomes[127].

Hence, ARL15 emerges as an important host factor for IAV, with an unidentified role both in the context of IAV infection as well as in the cell in general. ARL15 expression did not change throughout the course of infection with three viral strains (figures 3.7 in Results and S5 in supplementary data). This result is in agreement with the broad understanding that ARFs are regulated at a downstream level through activation/inactivation cycles[102,116]. In agreement, ARL15 subcellular localization changed during infection as observed by immunofluorescence (figure 3.8). In uninfected cells, ARL15 accumulated mostly at the cis-Golgi, co-localizing with GBF1, and was also found in cellular projections. Upon infection, ARL15 re-localized from the cis-Golgi and cell edges to cytoplasmic distinctive puncta that have not yet been identified. The change in distribution occurred early in infection and was maintained until 10 hours post-infection, but failed to co-localize with vRNP vesicles. Moreover, GBF1 accumulation was consistently perinuclear throughout infection. GBF1 is an ARF-GEF protein that initiates the coating of nascent vesicles from the cis-Golgi in the early secretory pathway and has been implicated

in the replication of many RNA viruses[152–155]. Slight changes observed in GBF1 pattern can be explained by Golgi morphological alterations known to occur during IAV infection[156]. Interestingly, the distribution of the non-functional ARL15-GFP expressed in the stable cell line did not change during infection, being present in the perinuclear area and in cell projections. These differences strongly support that ARL15 is relocated during IAV infection to the vicinity of aggregates to perform an undescribed function.

Initially, we sought to understand the point at which ARL15 was involved in vRNP trafficking. The early exit of ARL15 from GBF1-positive locations observed in figure 3.8a and quantified in figure 3.8b, supported a role of ARL15 in the initial steps of infection, for instance, in the transport of vRNPs to the nucleus (hypothesis 1 in figure 4.1). Alternatively, the close proximity of ARL15 to vRNP aggregates, likewise justified its involvement at later stages of infection (hypothesis 2 in figure 4.1). Both theories presented in figure 4.1 are not mutually exclusive. In fact, CD81 was reported to affect viral uncoating in the early steps of viral infection as well as to impact the budding of IAV particles[94].

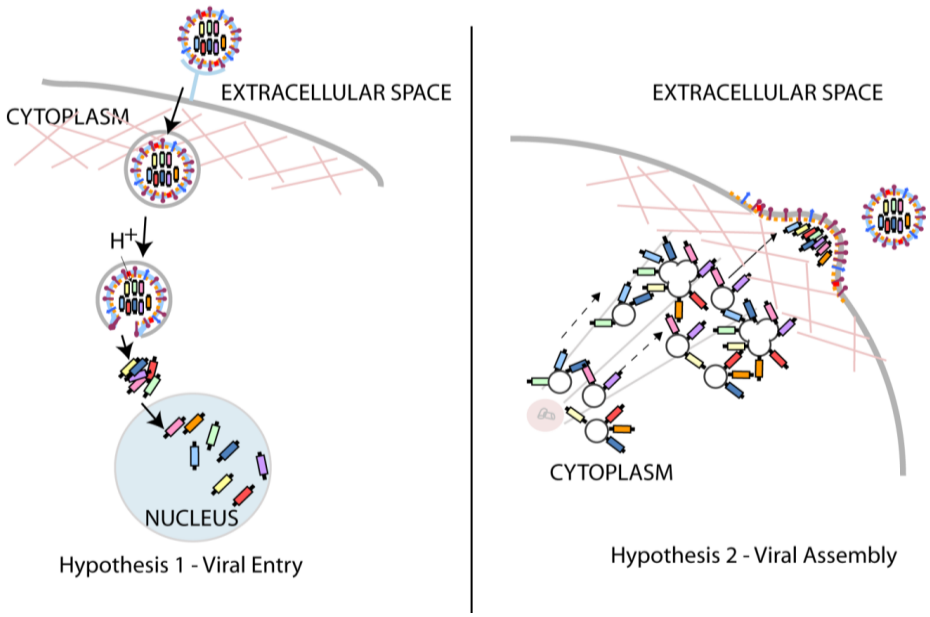

Figure 4.1. Predicted outcomes for depletion of ARL15. Hypothesis 1: ARL15 could affect the initial steps in viral infection such as receptor bindind, internalization, fusion to endosomes, nuclear import or, **Hypothesis 2**: ARL15 could affect steps in viral assembly, such as accumulation of vRNPs at the microtubule-organizing center, loading onto Rab11 vesicles, trafficking of vesicles throughout the recycling endossome. Illustration by MJ Amorim, unpublished.

To discriminate between the two hypotheses, ARL15 was depleted from cells and the effects on vRNP trafficking were observed. Results indicate that ARL15 functions in late stages of infection, as removing it did not affect vRNP entry into the nucleus, NP expression (figure 3.2, siNT vs siARL15 lanes) or vRNP loading on Rab11 vesicles. The latter observation is substantiated by reports describing that vRNP loading onto Rab11-positive vesicles, resulted in a punctate cytoplasmic distribution of NP, whose size increased during infection[70,79,131–133] [Costa SV *et al* 2015, unpublished]. Depletion of Rab11 caused a failure in this loading process, resulting in a dispersed distribution of NP throughout the cytoplasm[70]. The absence of ARL15 not only resulted in the cytoplasmic accumulation of distinct puncta but also in their enlargement, suggesting that ARL15 plays a role in vRNP transport. At this stage we can only suppose that these enlarged vesicles contain Rab11, an assumption substantiated by the fact that appearance of puncta is dependent on Rab11[79].

The enlargement of vRNP-containing puncta upon ARL15 depletion is an interesting feature that we are yet to clarify. Enlargement of vesicular size presumes that Rab11 vesicles are transitory platforms for vRNP transport to the assembly sites. In agreement, this concept is supported by the following observations: 1) Rab11 is found in minimal amounts inside virions[157,158], 2) Rab11 fails to co-localize with vRNPs at the plasma membrane[30,132], and 3) vRNPs do not present a head-to-tail orientation inside a virion, implicating, at least a partial vRNP-Rab11 detachment, resulting in an up-side-down organization of segments[159]. The vesicular enlargement observed in the absence of ARL15 could result from disturbing the transitory staging at two levels: 1) by leading to an increased loading of vRNPs on Rab11 vesicles (Pre-loading hypothesis in figure 4.2); or 2)a failure in a final yet uncharacterised step occurring subsequently to the staging area (Post-loading hypothesis in figure 4.2). We explored the involvement of ARL15 in vRNP recruitment by Rab11 via the artificial targeting of the Rab 11 to the mitochondria. Our premise was that if ARL15 were to be involved in loading of vRNPs onto Rab11 vesicles described in the ‘Pre-loading hypothesis’, overexpressing ARL15 would result in vRNP increase in the mitochondria, and the contrary would be observed if ARL15 promoted vRNP dissociation, or competed with Rab11 for vRNP binding. We observed that MitoRab11-WT binding to vRNPs was significantly reduced when ARL15 was present (figure 3.11). In this case, vRNPs distributed between the mitochondria and the cytoplasm.

Importantly, ARL15 did not localize at the mitochondria in the presence of either Rab11-WT or DN, indicating that the protein does not bind directly to Rab11 and does not compete for vRNP binding. This is also corroborated by the lack of ARL15 in vRNP-Rab11 aggregates during infection (figure 3.6). Altogether, it is possible that ARL15 influences the trafficking of Rab11-vRNP vesicles by contributing to the inactivation of Rab11 at later stages of infection, promoting the final delivery of vRNPs to the plasma membrane.

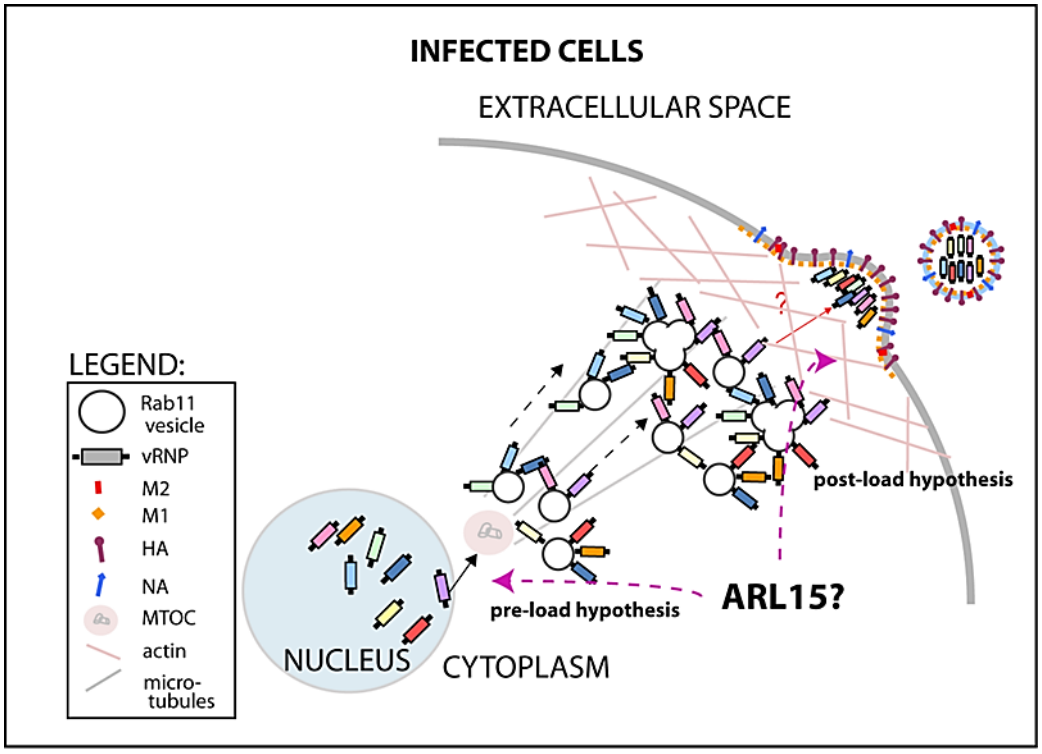

Figure 4.2. Predicted outcomes for the role of ARL15 during vRNP trafficking. Pre-loading hypothesis: ARL15 avoids overloading of the RE with vRNPS by switching of Rab11, promoting affluent transport towards the plasma membrane. Post-loading h**ypothesis:** ARL15 may faccilitate the transfer of vRNPs to the assembly sites by unloading the vesicles and switching off Rab11. Illustration by MJ Amorim, unpublished.

In agreement, experiments from our group suggest that vesicular increase is observed after overexpression of a constitutively active (CA) form of Rab11, and this increase is accompanied by a decrease in virion production. This observation supports the existence of an additional step that requires switching-off Rab11 for efficient vRNP delivery to the plasma membrane [Costa SV *et al* 2015, unpublished]. Furthermore, Eisfeld et al., had already suggested that the vRNP-Rab11 interaction could be disrupted prior to virion budding, perhaps via vRNP recruitment by the viral proteins M1-M2 associated at the

plasma membrane[132]. Overall this work supports the model of vRNP-Rab11 disruption, as ARL15 depletion contributed to the formation of enlarged cytoplasmic vRNP-carrying vesicles and decreased viral titers. Finally, it is becoming accepted that the intermediate staging area works as a platform to promote the interactions between 8 different vRNPs that are necessary to form a viral particle[74,81]. In this case, ARL15 might contribute to infection at this stage. At the present we can only speculate on its role but favor two theories: 1) ARL15 might be involved in the delivery of vRNPs to the plasma membrane or 2) might facilitate retrograde transport of Rab11 to the TGN to load more vRNPs. Be as it may, ARL15 was not found in virions and therefore must not be the final acceptor of vRNPs[157].

Our working hypotheses revolve around mechanisms affecting vRNP transport. However, it is equally possible that ARL15 affects other steps in viral infection that we fail to investigate during this thesis. Initial steps seem to operate normally; however, the quantification of viral transcription and replication rates as well as the evaluation of viral protein expression, beyond NP, are crucial to fully characterize the role of ARL15. Similarly, it might influence trafficking of the remaining virion components, including for example M1, M2, HA and NA. Quantification of the three transmembrane proteins at the cell surface by flow cytometry is necessary to discard this hypothesis, as the measurement of M1 levels, beneath the plasma membrane or inside virions, would provide evidence concerning ARL15 involvement in M1 trafficking.

In conclusion, this thesis shows evidence that ARL15 is an important host protein that facilitates vRNP traffic at late stages of IAV infection. Its intracellular distribution is sensitive to infection and its absence results in deficient transport of vesicles carrying the vRNPs, leading to their accumulation in the cytoplasm. Furthermore, our data shows that ARL15 significantly disturbs the binding of vRNPs to Rab11, indicating that it may contribute to a yet uncharacterized Rab11 inactivation step before vRNPs reach the membrane. However, these constitute the initial steps of ARL15 characterization in the viral lifecycle. In the future, complementary studies should assess the consequences of targeting this pathway for antiviral therapy.

CHAPTER 5 | Future perspectives

The data herein presented revealed that ARL15 positively influences IAV infection presumably by disturbing the interaction between the viral genome and small GTPase Rab11 and aiding in vRNP transfer to the plasma membrane for budding. However, ARL15 characterization remains incomplete either in context of infected or uninfected cells. To complete this study with the following analysis would be required.

Firstly, not much is known about the role of ARL15 in the normal cell. Biochemical, imaging and genetic assays should be used to evaluate the intracellular localization, catalytic activity and regulation mechanisms of ARL15, determining important domains for the predicted function of the protein and putative associations with cellular membranes.

Secondly, the role of ARL15 during IAV infection lacks characterization. The study herein presented does not elucidate in detail the relation between ARL15 and Rab11. One way to explore such interaction could be to perform pull down assays evaluating the outcomes of vRNP-Rab11 ligation in the presence of ARL15, by using the already established HEK 293T cell lines expressing WT, CA and DN forms of Rab11. Likewise, it would be of interest to analyze biochemically whether ARL15 binds the Rab small GTPase or any of its identified interacting proteins. Alternatively, one could analyze the effects on viral production after supplementing Rab11-WT and ARL15, for which a dominant negative form of Rab11 could be used as control.

Thirdly, the lack of co-localization of ARL15 with GBF1 should be further investigated, namely the identification of ARL15 compartment in infection and molecular mechanisms underlying this change.

Fourthly, the effects of ARL15 depletion on other viral steps should be analyzed, mostly due to the importance of ARLs in regulating trafficking pathways. In this sense, the intracellular transport of other proteins such as HA, NA and M2 should be assessed by flow cytometry, as these proteins reach the plasma membrane via the classical secretory pathway. In parallel, the distribution of M1 and its role in the particle assembly should also be evaluated in the presence or absence of ARL15. The involvement of viral M1 in the later stages of infection is poorly understood. It is supposed that M1 binds the cytoplasmic tail of M2 and aids vRNP packaging at the plasma membrane[34]. Thus, the interaction between M1 and M2 in the absence of ARL15 would constitute an important assay

elucidating this particular step. In addition to the trafficking of viral components, particle budding and the ultrastructure of virions should also be evaluated as a measure of efficiency in the very last step of infection, which could be easily accomplished by electron microscopy.

Finally, the studies proposed so far include tissue cultured cells resorting to siRNA treatments to deplete ARL15 that are useful but not devoid of limitations. In order to study infection *in vivo* in cells without ARL15 we have started the process of establishing ARL15 knock-out mice, using the CRISPR-Cas9 system. This procedure was initiated during the course of my internship. My contribution was to clone an ARL15 sequence fused to a guide RNA, with the purpose of coding the RNA segment responsible for guiding the nuclease to the target ARL15 gene. Mouse embryonic fibroblast cells, permissive to IAV infection, will be isolated from these mice and used to corroborate all the observations achieved so far as well as used to validate biochemical assays previously performed. Additionally, these knock out mice are invaluable to characterize the effect of ARL15 on viral pathogenesis, immune response and inflammation.

CHAPTER 6 | References

1. Collier, L., Kellam, P. & Oxford, J. Human virology. *Hum. Virol.* (2011).
2. Lamb, R., Krug, R. & Knipe, D. Fields virology. *Fields Virol.* **1445,** 1996 (2001).
3. Webster, R. G., Bean, W. J., Gorman, O. T., Chambers, T. M. & Kawaoka, Y. Evolution and ecology of influenza A viruses. *Microbiol. Rev.* **56,** 152–179 (1992).
4. Transmission of Influenza Viruses from Animals to People | Seasonal Influenza (Flu) | CDC. at <http://www.cdc.gov/flu/about/viruses/transmission.htm>
5. Kuiken, T. *et al.* Host species barriers to influenza virus infections. *Science* **312,** 394–397 (2006).
6. Webster, R. G., Peiris, M., Chen, H. & Guan, Y. H5N1 outbreaks and enzootic influenza. *Emerg. Infect. Dis.* **12,** 3–8 (2006).
7. Horby, P. H7N9 is a virus worth worrying about. *Nature* 2013 (2013). doi:10.1038/496399a
8. Tognotti, E. Influenza pandemics: a historical retrospect. *J. Infect. Dev. Ctries.* **3,** 331–334 (2009).
9. Koel, B. F. *et al.* Substitutions near the receptor binding site determine major antigenic change during influenza virus evolution. *Science* **342,** 976–9 (2013).
10. Bouvier, N. M. & Palese, P. The biology of influenza viruses. *Vaccine* **26,** D49–D53 (2008).
11. Influenza remains a threat. at <http://ecdc.europa.eu/en/healthtopics/seasonal_influenza/key_messages/Pages/key_messages_2.aspx>
12. Reed, C., Meltzer, M. I., Finelli, L. & Fiore, A. Public health impact of including two lineages of influenza B in a quadrivalent seasonal influenza vaccine. *Vaccine* **30,** 1993–1998 (2012).
13. Peiris, M. *et al.* Human infection with influenza H9N2. *Lancet* **354,** 916–917 (1999).
14. Stegeman, A. *et al.* Avian influenza A virus (H7N7) epidemic in The Netherlands in 2003: course of the epidemic and effectiveness of control measures. *J. Infect. Dis.* **190,** 2088–2095 (2004).
15. Tweed, S. A. *et al.* Human illness from avian influenza H7N3, British Columbia. *Emerg. Infect. Dis.* **10,** 2196–9 (2004).
16. Cheng, V. C. C., To, K. K. W., Tse, H., Hung, I. F. N. & Yuen, K.-Y. Two years after pandemic influenza A/2009/H1N1: what have we learned? *Clin. Microbiol. Rev.* **25,** 223–63 (2012).
17. Carrat, F. & Flahault, A. Influenza vaccine: The challenge of antigenic drift. *Vaccine* **25,** 6852–6862 (2007).
18. Jefferson, T. Influenza vaccination: policy versus evidence. *BMJ Br. Med. J.* **333,** 912–915 (2006).
19. Protection from Flu Vaccination Reduced this Season | CDC Online Newsroom | CDC. at <http://www.cdc.gov/media/releases/2015/p0115-flu-vaccination.html>
20. Selecting the Viruses in the Seasonal Influenza (Flu) Vaccine | Health Professionals | Seasonal Influenza (Flu). at <http://www.cdc.gov/flu/professionals/vaccination/virusqa.htm>
21. Global circulation of influenza. at <http://gamapserver.who.int/gareports/Default.aspx?ReportNo=10>
22. Chambers, B. S., Parkhouse, K., Ross, T. M., Alby, K. & Hensley, S. E. Identification of Hemagglutinin Residues Responsible for H3N2 Antigenic Drift during the 2014–2015 Influenza Season. *Cell Rep.* **12,** 1–6 (2015).
23. HAN Archive - 00374|Health Alert Network (HAN). at <http://emergency.cdc.gov/han/han00374.asp>
24. Ison, M. G. Antivirals and resistance: Influenza virus. *Curr. Opin. Virol.* **1,** 563–573 (2011).
25. Mizuta, K. *et al.* Epidemics of two Victoria and Yamagata influenza B lineages in Yamagata, Japan. *Epidemiol. Infect.* **132,** 721–726 (2004).

26. Osterhaus, A. D. Influenza B Virus in Seals. *Science (80-.).* **288,** 1051–1053 (2000).
27. Matsuzaki, Y. *et al.* Genetic diversity of influenza B virus: The frequent reassortment and cocirculation of the genetically distinct reassortant viruses in a community. *J. Med. Virol.* **74,** 132–140 (2004).
28. Katagiri, S., Ohizumi, A. & Homma, M. An outbreak of type C influenza in a children's home. *J. Infect. Dis.* **148,** 51–56 (1983).
29. Horimoto, T. & Kawaoka, Y. Influenza: lessons from past pandemics, warnings from current incidents. *Nat. Rev. Microbiol.* **3,** 591–600 (2005).
30. Eisfeld, A. J., Neumann, G. & Kawaoka, Y. At the centre: influenza A virus ribonucleoproteins. *Nat. Rev. Microbiol.* **13,** 28–41 (2014).
31. Noda, T. *et al.* Architecture of ribonucleoprotein complexes in influenza A virus particles. *Nature* **439,** 490–492 (2006).
32. Nayak, D. P., Hui, E. K.-W. W. & Barman, S. Assembly and budding of influenza virus. *Virus Res.* **106,** 147–165 (2004).
33. Boulo, S., Akarsu, H., Ruigrok, R. W. H. & Baudin, F. Nuclear traffic of influenza virus proteins and ribonucleoprotein complexes. *Virus Res.* **124,** 12–21 (2007).
34. Rossman, J. & Lamb, R. Influenza virus assembly and budding. *Virology* **411,** 229–236 (2011).
35. Neumann, G., Brownlee, G. G., Fodor, E. & Kawaoka, Y. Orthomyxovirus replication, transcription, and polyadenylation. *Curr. Top. Microbiol. Immunol.* **283,** 121–143 (2004).
36. Influenza A virus (ID 10290) - Genome - NCBI. at <http://www.ncbi.nlm.nih.gov/genome/?term=txid211044>
37. Wise, H. M. *et al.* Identification of a Novel Splice Variant Form of the Influenza A Virus M2 Ion Channel with an Antigenically Distinct Ectodomain. *PLoS Pathog.* **8,** (2012).
38. Skehel, J. J. & Wiley, D. C. Receptor Binding And Membrane Fusion In Virus Entry : The Influenza Hemagglutinin. *Annu. Rev. Biochem.* **69,** 531 – 569 (2000).
39. Rust, M. J., Lakadamyali, M., Zhang, F. & Zhuang, X. Assembly of endocytic machinery around individual influenza viruses during viral entry. *Nat. Struct. Mol. Biol.* **11,** 567–573 (2004).
40. Sun, X. & Whittaker, G. R. Role of the actin cytoskeleton during influenza virus internalization into polarized epithelial cells. *Cell. Microbiol.* **9,** 1672–1682 (2007).
41. De Conto, F. *et al.* Highly dynamic microtubules improve the effectiveness of early stages of human influenza A/NWS/33 virus infection in LLC-MK2 cells. *PLoS One* **7,** (2012).
42. Huang, Q. *et al.* Early steps of the conformational change of influenza virus hemagglutinin to a fusion active state: Stability and energetics of the hemagglutinin. *Biochim. Biophys. Acta - Biomembr.* **1614,** 3–13 (2003).
43. Pinto, L. H., Holsinger, L. J. & Lamb, R. A. Influenza virus M2 protein has ion channel activity. *Cell* **69,** 517–528 (1992).
44. Banerjee, I. *et al.* Influenza A virus uses the aggresome processing machinery for host cell entry. *Science* **346,** 473–7 (2014).
45. Chu, V. C. & Whittaker, G. R. Influenza virus entry and infection require host cell N-linked glycoprotein. *Proc. Natl. Acad. Sci. U. S. A.* **101,** 18153–8 (2004).
46. O'Neill, R. E., Jaskunas, R., Blobel, G., Palese, P. & Moroianu, J. Nuclear import of influenza virus RNA can be mediated by viral nucleoprotein and transport factors required for protein import. *J. Biol. Chem.* **270,** 22701–22704 (1995).
47. Hutchinson, E. C. & Fodor, E. Nuclear import of the influenza A virus transcriptional machinery. *Vaccine* **30,** 7353–7358 (2012).
48. Amorim, M. J. & Digard, P. Influenza A virus and the cell nucleus. *Vaccine* **24,** 6651–5 (2006).
49. Hay, A. J., Lomniczi, B., Bellamy, A. R. & Skehel, J. J. Transcription of the influenza virus genome. *Virology* **83,** 337–355 (1977).
50. Hay, A. J. & Skehel, J. J. Characterization of influenza virus RNA transcripts synthesized in vitro. *J. Gen. Virol.* **44,** 599–608 (1979).
51. Dias, A. *et al.* The cap-snatching endonuclease of influenza virus polymerase resides in the PA subunit. *Nature* **458,** 914–918 (2009).

52. Poon, L. L., Pritlove, D. C., Fodor, E. & Brownlee, G. G. Direct evidence that the poly(A) tail of influenza A virus mRNA is synthesized by reiterative copying of a U track in the virion RNA template. *J. Virol.* **73,** 3473–3476 (1999).
53. Robertson, J. S., Schubert, M. & Lazzarini, R. A. Polyadenylation sites for influenza virus mRNA. *J. Virol.* **38,** 157–163 (1981).
54. Poon, L. L., Pritlove, D. C., Sharps, J. & Brownlee, G. G. The RNA polymerase of influenza virus, bound to the 5' end of virion RNA, acts in cis to polyadenylate mRNA. *J. Virol.* **72,** 8214–8219 (1998).
55. Fodor, E. The RNA polymerase of influenza A virus: Mechanisms of viral transcription and replication. *Acta Virol.* **57,** 113–122 (2013).
56. Krumbholz, A. *et al.* Current knowledge on PB1-F2 of influenza A viruses. *Med. Microbiol. Immunol.* **200,** 69–75 (2011).
57. Jagger, B. W. *et al.* An Overlapping Protein-Coding Region in Influenza A Virus Segment 3 Modulates the Host Response. *Science (80-.).* **337,** 199–204 (2012).
58. Muramoto, Y., Noda, T., Kawakami, E., Akkina, R. & Kawaoka, Y. Identification of novel influenza A virus proteins translated from PA mRNA. *J. Virol.* **87,** 2455–62 (2013).
59. ViralZone: Influenzavirus A. at <http://viralzone.expasy.org/all_by_species/6.html>
60. Noton, S. L. *et al.* Identification of the domains of the influenza A virus M1 matrix protein required for NP binding, oligomerization and incorporation into virions. *J. Gen. Virol.* **88,** 2280–2290 (2007).
61. Akarsu, H. *et al.* Crystal structure of the M1 protein-binding domain of the influenza A virus nuclear export protein (NEP/NS2). *EMBO J.* **22,** 4646–4655 (2003).
62. Elton, D. *et al.* Interaction of the influenza virus nucleoprotein with the cellular CRM1-mediated nuclear export pathway. *J. Virol.* **75,** 408–419 (2001).
63. Whittaker, G. R. & Helenius, A. Nuclear import and export of viruses and virus genomes. *Virology* **246,** 1–23 (1998).
64. Bui, M., Wills, E. G., Helenius, A. & Whittaker, G. R. Role of the influenza virus M1 protein in nuclear export of viral ribonucleoproteins. *J. Virol.* **74,** 1781–1786 (2000).
65. Chua, M. A., Schmid, S., Perez, J. T., Langlois, R. A. & tenOever, B. R. Influenza A Virus Utilizes Suboptimal Splicing to Coordinate the Timing of Infection. *Cell Rep.* **3,** 23–29 (2013).
66. Lamb, R. A., Choppin, P. W., Chanock, R. M. & Lai, C. J. Mapping of the two overlapping genes for polypeptides NS1 and NS2 on RNA segment 8 of influenza virus genome. *Proc. Natl. Acad. Sci. U. S. A.* **77,** 1857–1861 (1980).
67. Robb, N. C., Jackson, D., Vreede, F. T. & Fodor, E. Splicing of influenza A virus NS1 mRNA is independent of the viral NS1 protein. *J. Gen. Virol.* **91,** 2331–2340 (2010).
68. Talon, J. *et al.* Activation of interferon regulatory factor 3 is inhibited by the influenza A virus NS1 protein. *J. Virol.* **74,** 7989–7996 (2000).
69. Moeller, A., Kirchdoerfer, R. N., Potter, C. S., Carragher, B. & Wilson, I. a. Organization of the influenza virus replication machinery. *Science* **338,** 1631–4 (2012).
70. Amorim, M. J. *et al.* A Rab11- and microtubule-dependent mechanism for cytoplasmic transport of influenza A virus viral RNA. *J. Virol.* **85,** 4143–56 (2011).
71. Kawaguchi, A., Matsumoto, K. & Nagata, K. YB-1 Functions as a Porter To Lead Influenza Virus Ribonucleoprotein Complexes to Microtubules. *J. Virol.* **86,** 11086–11095 (2012).
72. Kao, R. Y. *et al.* Identification of influenza A nucleoprotein as an antiviral target. *Nat. Biotechnol.* **28,** 600–605 (2010).
73. Amorim, M. J., Kao, R. Y. & Digard, P. Nucleozin targets cytoplasmic trafficking of viral ribonucleoprotein-Rab11 complexes in influenza A virus infection. *J. Virol.* **87,** 4694–703 (2013).
74. Hutchinson, E. C., von Kirchbach, J. C., Gog, J. R. & Digard, P. Genome packaging in influenza A virus. *J. Gen. Virol.* **91,** 313–328 (2010).
75. Bancroft, C. T. & Parslow, T. G. Evidence for segment-nonspecific packaging of the influenza a virus genome. *J. Virol.* **76,** 7133–7139 (2002).

76. Enami, M., Sharma, G., Benham, C. & Palese, P. An influenza virus containing nine different RNA segments. *Virology* **185,** 291–298 (1991).
77. Hatada, E. & Hasegawa, M. Control of influenza virus gene expression: quantitative analysis of each viral RNA species in infected cells. *J. Biochem.* **105,** 537–546 (1989).
78. Bergmann, M. & Muster, T. The relative amount of an influenza A virus segment present in the viral particle is not affected by a reduction in replication of that segment. *J. Gen. Virol.* **76,** 3211–3215 (1995).
79. Chou, Y. ying *et al.* Colocalization of Different Influenza Viral RNA Segments in the Cytoplasm before Viral Budding as Shown by Single-molecule Sensitivity FISH Analysis. *PLoS Pathog.* **9,** (2013).
80. Lakdawala, S. S. *et al.* Influenza A Virus Assembly Intermediates Fuse in the Cytoplasm. *PLoS Pathog.* **10,** (2014).
81. Gerber, M., Isel, C., Moules, V. & Marquet, R. Selective packaging of the influenza A genome and consequences for genetic reassortment. *Trends Microbiol.* **22,** 446–455 (2014).
82. Suzuki, T. & Suzuki, Y. Virus infection and lipid rafts. *Biol. Pharm. Bull.* **29,** 1538–1541 (2006).
83. Leser, G. P. & Lamb, R. A. Influenza virus assembly and budding in raft-derived microdomains: A quantitative analysis of the surface distribution of HA, NA and M2 proteins. *Virology* **342,** 215–227 (2005).
84. Martin, K. & Helenius, A. Nuclear transport of influenza virus ribonucleoproteins: The viral matrix protein (M1) promotes export and inhibits import. *Cell* **67,** 117–130 (1991).
85. Chen, B. J., Leser, G. P., Jackson, D. & Lamb, R. A. The influenza virus M2 protein cytoplasmic tail interacts with the M1 protein and influences virus assembly at the site of virus budding. *J. Virol.* **82,** 10059–10070 (2008).
86. Chen, B. J., Leser, G. P., Morita, E. & Lamb, R. A. Influenza virus hemagglutinin and neuraminidase, but not the matrix protein, are required for assembly and budding of plasmid-derived virus-like particles. *J. Virol.* **81,** 7111–7123 (2007).
87. Ali, A., Avalos, R., Ponimaskin, E. & Nayak, D. Influenza virus assembly: effect of influenza virus glycoproteins on the membrane association of M1 protein. *J. Virol.* **74,** 8709–8719 (2000).
88. Ruigrok, R., Baudin, F., Petit, I. & Weissenhorn, W. Role of influenza virus M1 protein in the viral budding process. *Int. Congr. Ser.* **1219,** 397–404 (2001).
89. Rossman, J. S., Jing, X., Leser, G. P. & Lamb, R. A. Influenza Virus M2 Protein Mediates ESCRT-Independent Membrane Scission. *Cell* **142,** 902–913 (2010).
90. Gorai, T. *et al.* F1Fo-ATPase, F-type proton-translocating ATPase, at the plasma membrane is critical for efficient influenza virus budding. *Proc. Natl. Acad. Sci.* **109,** 4615–4620 (2012).
91. Liu, G. *et al.* Cofilin-1 is involved in regulation of actin reorganization during influenza A virus assembly and budding. *Biochem. Biophys. Res. Commun.* **453,** 821–5 (2014).
92. Demirov, D., Gabriel, G., Schneider, C., Hohenberg, H. & Ludwig, S. Interaction of influenza A virus matrix protein with RACK1 is required for virus release. *Cell. Microbiol.* **14,** 774–789 (2012).
93. Musiol, A. *et al.* Annexin A6-balanced late endosomal cholesterol controls influenza a replication and propagation. *MBio* **4,** (2013).
94. He, J. *et al.* Dual Function of CD81 in Influenza Virus Uncoating and Budding. *PLoS Pathog.* **9,** (2013).
95. Palese, P., Tobita, K., Ueda, M. & Compans, R. W. Characterization of temperature sensitive influenza virus mutants defective in neuraminidase. *Virology* **61,** 397–410 (1974).
96. Air, G. M. & Laver, W. G. The neuraminidase of influenza virus. *Proteins Struct. Funct. Genet.* **6,** 341–356 (1989).
97. Steinhauer, D. A. Role of hemagglutinin cleavage for the pathogenicity of influenza virus. *Virology* **258,** 1–20 (1999).
98. Chen, J. *et al.* Structure of the hemagglutinin precursor cleavage site, a determinant of influenza pathogenicity and the origin of the labile conformation. *Cell* **95,** 409–417 (1998).

99. Bruce, E. A., Digard, P. & Stuart, A. D. The Rab11 pathway is required for influenza A virus budding and filament formation. *J. Virol.* **84,** 5848–5859 (2010).
100. Welz, T., Wellbourne-Wood, J. & Kerkhoff, E. Orchestration of cell surface proteins by Rab11. *Trends Cell Biol.* **24,** 407–414 (2014).
101. Mellman, I. & Nelson, W. J. Coordinated protein sorting, targeting and distribution in polarized cells. *Nat. Rev. Mol. Cell Biol.* **9,** 833–845 (2008).
102. Takai, Y., Sasaki, T. & Matozaki, T. Small GTP-Binding Proteins. *Physiol Rev* **81,** 153–208 (2001).
103. Cherfils, J. & Zeghouf, M. Regulation of small GTPases by GEFs, GAPs, and GDIs. *Physiol. Rev.* **93,** 269–309 (2013).
104. Shin, H. W., Takatsu, H. & Nakayama, K. Mechanisms of membrane curvature generation in membrane traffic. *Membranes (Basel).* **2,** 118–133 (2012).
105. Bock, J. B., Matern, H. T., Peden, A. A. & Scheller, R. H. A genomic perspective on membrane compartment organization. *Nature* **409,** 839–841 (2001).
106. Stalder, D. & Antonny, B. Arf GTPase regulation through cascade mechanisms and positive feedback loops. *FEBS Lett.* **587,** 2028–2035 (2013).
107. Behnia, R. & Munro, S. Organelle identity and the signposts for membrane traffic. *Nature* **438,** 597–604 (2005).
108. Zerial, M. & McBride, H. Rab proteins as membrane organizers. *Nat. Rev. Mol. Cell Biol.* **2,** 107–117 (2001).
109. Kawasaki, M., Nakayama, K. & Wakatsuki, S. Membrane recruitment of effector proteins by Arf and Rab GTPases. *Curr. Opin. Struct. Biol.* **15,** 681–689 (2005).
110. Alenquer, M. & Amorim, M. Exosome Biogenesis, Regulation, and Function in Viral Infection. *Viruses* **7,** 5066–5083 (2015).
111. Wang, J., Morita, Y., Mazelova, J. & Deretic, D. The Arf GAP ASAP1 provides a platform to regulate Arf4- and Rab11–Rab8-mediated ciliary receptor targeting. *EMBO J.* **31,** 4057–4071 (2012).
112. Inoue, H., Ha, V. L., Prekeris, R. & Randazzo, P. A. Arf GTPase-activating protein ASAP1 interacts with Rab11 effector FIP3 and regulates pericentrosomal localization of transferrin receptor-positive recycling endosome. *Mol. Biol. Cell* **19,** 4224–4237 (2008).
113. Martin, A. *et al.* Activation of phospholipase D and phosphatidylinositol 4-phosphate 5- kinase in HL60 membranes is mediated by endogenous Arf but not Rho. *J. Biol. Chem.* **271,** 17397–17403 (1996).
114. ADP-ribosylation factor (ARF) family GTPases Gene Family | HUGO Gene Nomenclature Committee. at <http://www.genenames.org/cgi-bin/genefamilies/set/357>
115. Donaldson, J. G. & Jackson, C. L. ARF family G proteins and their regulators: roles in membrane transport, development and disease. *Nat. Rev. Mol. Cell Biol.* **12,** 362–375 (2011).
116. Gillingham, A. K. & Munro, S. The small G proteins of the Arf family and their regulators. *Annu. Rev. Cell Dev. Biol.* **23,** 579–611 (2007).
117. Kahn, R. A. & Gilman, A. G. Purification of a protein cofactor required for ADP-ribosylation of the stimulatory regulatory component of adenylate cyclase by cholera toxin. *J. Biol. Chem.* **259,** 6228–6234 (1984).
118. Kahn, R. A. *et al.* Nomenclature for the human Arf family of GTP-binding proteins: ARF, ARL, and SAR proteins. *J. Cell Biol.* **172,** 645–650 (2006).
119. Pasqualato, S., Renault, L. & Cherfils, J. Arf, Arl, Arp and Sar proteins: a family of GTP-binding proteins with a structural device for 'front-back' communication. *EMBO Rep.* **3,** 1035–41 (2002).
120. Antonny, B., Beraud-Dufour, S., Chardin, P. & Chabre, M. N-terminal hydrophobic residues of the G-protein ADP-ribosylation factor-1 insert into membrane phospholipids upon GDP to GTP exchange. *Biochemistry* **36,** 4675–4684 (1997).
121. Pasqualato, S., Ménétrey, J., Franco, M. & Cherfils, J. The structural GDP/GTP cycle of human Arf6. *EMBO Rep.* **2,** 234–238 (2001).

122. Macia, E. *et al.* The GDP-bound form of Arf6 is located at the plasma membrane. *J. Cell Sci.* **117,** 2389–2398 (2004).
123. Donaldson, J. G. & Honda, A. Localization and function of Arf family GTPases. *Biochem. Soc. Trans.* **33,** 639–642 (2005).
124. Bhamidipati, A., Lewis, S. A. & Cowan, N. J. ADP ribosylation factor-like protein 2 (Arl2) regulates the interaction of tubulin-folding cofactor D with native tubulin. *J. Cell Biol.* **149,** 1087–1096 (2000).
125. Tian, G., Thomas, S. & Cowan, N. J. Effect of TBCD and its regulatory interactor Arl2 on tubulin and microtubule integrity. *Cytoskeleton* **67,** 706–714 (2010).
126. Zhou, C., Cunningham, L., Marcus, A. I., Li, Y. & Kahn, R. A. Arl2 and Arl3 regulate different microtubule-dependent processes. *Mol. Biol. Cell* **17,** 2476–2487 (2006).
127. Rosa-Ferreira, C. & Munro, S. Arl8 and SKIP Act Together to Link Lysosomes to Kinesin-1. *Dev. Cell* **21,** 1171–1178 (2011).
128. Carrasco, M., Amorim, M. J. & Digard, P. Lipid raft-dependent targeting of the influenza A virus nucleoprotein to the apical plasma membrane. *Traffic* **5,** 979–92 (2004).
129. De Wit, E. *et al.* Efficient generation and growth of influenza virus A/PR/8/34 from eight cDNA fragments. in *Virus Res.* **103,** 155–161 (2004).
130. Matrosovich, M., Matrosovich, T., Garten, W. & Klenk, H.-D. New low-viscosity overlay medium for viral plaque assays. *Virol. J.* **3,** 63 (2006).
131. Momose, F. *et al.* Apical transport of influenza A virus ribonucleoprotein requires Rab11-positive recycling endosome. *PLoS One* **6,** (2011).
132. Eisfeld, A. J., Kawakami, E., Watanabe, T., Neumann, G. & Kawaoka, Y. RAB11A is essential for transport of the influenza virus genome to the plasma membrane. *J. Virol.* **85,** 6117–6126 (2011).
133. Avilov, S. V., Moisy, D., Naffakh, N. & Cusack, S. Influenza A virus progeny vRNP trafficking in live infected cells studied with the virus-encoded fluorescently tagged PB2 protein. *Vaccine* **30,** 7411–7417 (2012).
134. Jackson, A. L. & Linsley, P. S. Recognizing and avoiding siRNA off-target effects for target identification and therapeutic application. *Nat. Rev. Drug Discov.* **9,** 57–67 (2010).
135. Fedorov, Y. *et al.* Off-target effects by siRNA can induce toxic phenotype. *RNA* **12,** 1188–1196 (2006).
136. Richards, J. B. *et al.* A genome-wide association study reveals variants in ARL15 that influence adiponectin levels. *PLoS Genet.* **5,** e1000768 (2009).
137. Li, Y. *et al.* Association study of ARL15 and CDH13 with T2DM in a Han Chinese population. *Int. J. Med. Sci.* **11,** 522–7 (2014).
138. Negi, S. *et al.* A genome-wide association study reveals ARL15, a novel non-HLA susceptibility gene for rheumatoid arthritis in North Indians. *Arthritis Rheum.* **65,** 3026–35 (2013).
139. Tissue expression of ARL15 - Summary - The Human Protein Atlas. at <http://www.proteinatlas.org/ENSG00000185305-ARL15/tissue>
140. ExoCarta: Gene summary. at <http://www.exocarta.org/gene_summary?gene_id=54622>
141. Gonzales, P. A. *et al.* Large-scale proteomics and phosphoproteomics of urinary exosomes. *J. Am. Soc. Nephrol.* **20,** 363–379 (2009).
142. Wang, Z., Hill, S., Luther, J. M., Hachey, D. L. & Schey, K. L. Proteomic analysis of urine exosomes by multidimensional protein identification technology (MudPIT). *Proteomics* **12,** 329–38 (2012).
143. Liang, B. *et al.* Characterization and proteomic analysis of ovarian cancer-derived exosomes. *J. Proteomics* **80,** 171–82 (2013).
144. Prunotto, M. *et al.* Proteomic analysis of podocyte exosome-enriched fraction from normal human urine. *J. Proteomics* **82,** 193–229 (2013).
145. Principe, S. *et al.* In-depth proteomic analyses of exosomes isolated from expressed prostatic secretions in urine. *Proteomics* **13,** 1667–1671 (2013).
146. Aridor, M. & Hannan, L. A. Traffic jam: a compendium of human diseases that affect intracellular transport processes. *Traffic* **1,** 836–851 (2000).

147. Cohen, L. A. & Donaldson, J. G. Analysis of Arf GTP-binding protein function in cells. *Curr. Protoc. Cell Biol.* (2010). doi:10.1002/0471143030.cb1412s48
148. Karlas, A. *et al.* Genome-wide RNAi screen identifies human host factors crucial for influenza virus replication. *Nature* **463,** 818–822 (2010).
149. König, R. *et al.* Human host factors required for influenza virus replication. *Nature* **463,** 813–817 (2010).
150. Watanabe, T., Watanabe, S. & Kawaoka, Y. Cellular networks involved in the influenza virus life cycle. *Cell Host Microbe* **7,** 427–439 (2010).
151. Shapira, S. D. *et al.* A Physical and Regulatory Map of Host-Influenza Interactions Reveals Pathways in H1N1 Infection. *Cell* **139,** 1255–1267 (2009).
152. Goueslain, L. *et al.* Identification of GBF1 as a cellular factor required for hepatitis C virus RNA replication. *J. Virol.* **84,** 773–787 (2010).
153. Carpp, L. N., Rogers, R. S., Moritz, R. L. & Aitchison, J. D. Quantitative proteomic analysis of host-virus interactions reveals a role for Golgi brefeldin A resistance factor 1 (GBF1) in dengue infection. *Mol. Cell. Proteomics* **13,** 2836–54 (2014).
154. Belov, G. A., Kovtunovych, G., Jackson, C. L. & Ehrenfeld, E. Poliovirus replication requires the N-terminus but not the catalytic Sec7 domain of ArfGEF GBF1. *Cell. Microbiol.* **12,** 1463–1479 (2010).
155. Lanke, K. H. W. *et al.* GBF1, a guanine nucleotide exchange factor for Arf, is crucial for coxsackievirus B3 RNA replication. *J. Virol.* **83,** 11940–11949 (2009).
156. Brydon, E. W. A., Smith, H. & Sweet, C. Influenza A virus-induced apoptosis in bronchiolar epithelial (NCl-H292) cells limits pro-inflammatory cytokine release. *J. Gen. Virol.* **84,** 2389–2400 (2003).
157. Shaw, M. L., Stone, K. L., Colangelo, C. M., Gulcicek, E. E. & Palese, P. Cellular proteins in influenza virus particles. *PLoS Pathog.* **4,** e1000085 (2008).
158. Hutchinson, E. C. *et al.* Conserved and host-specific features of influenza virion architecture. *Nat. Commun.* **5,** 4816 (2014).
159. Sugita, Y., Sagara, H., Noda, T. & Kawaoka, Y. Configuration of viral ribonucleoprotein complexes within the influenza A virion. *J. Virol.* **87,** 12879–84 (2013).

CHAPTER 7 | Supplementary Data

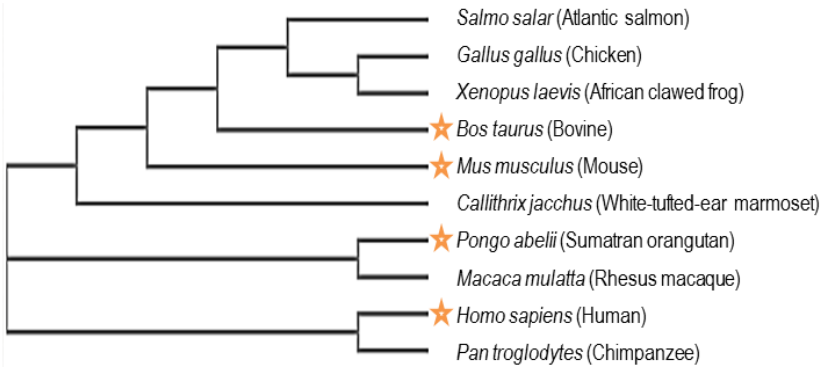

Figure S1. Homology tree of ARL15 of chordate species. Sequences retrieved from Uniprot© database, alligned using Clustal Omega to produce the homology tree output. Stars highlight sequences that were manually annotated. The remaining sequences were processed by TREMBL. The overall aminoacid sequence identity is of 63%. The aminoacid sequence identity of starred sequences is of 93%. Uniprot references of ARL15 sequences: Ss: C0HAE3; Gg:F1NMW9; Xl: Q6DJE1; Bt: Q5EA19; Mmusculus: Q8BGR6; Cj: U3EFB9; Pa: Q5RFN0; Mmulata: H9ESN0; Hs: Q9NXU5; Pt: K7AXD4.

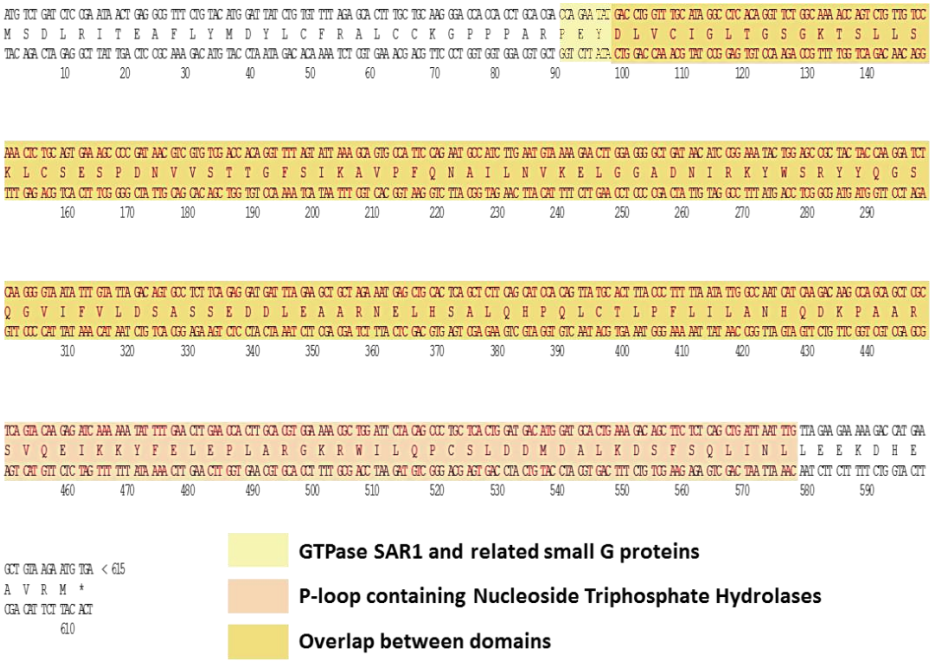

Figure S2. ARL15 anotation. Sense and antisense coding sequences, and correspondant translation of ARL15 protein (NP_061960.1). Information retrieved from the National Center for Biotechnology Information (NCBI©) database. Prediction of major domains, common to SAR1 protein.

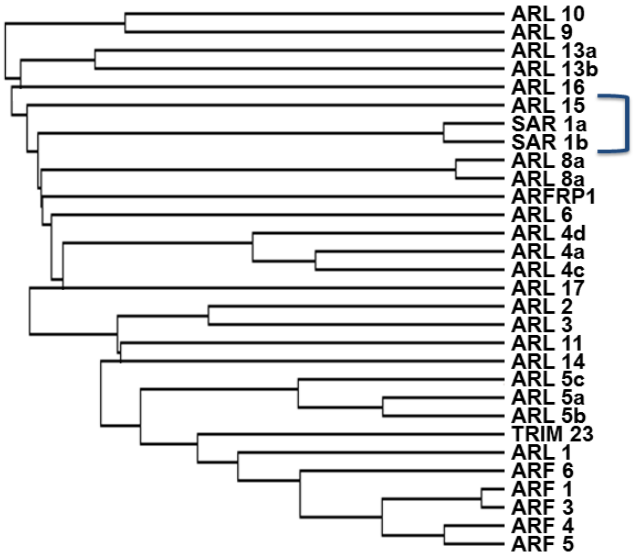

Figure S3. Homology tree with members of the human ARF-family. Identity: 0.3%. Sequences retrieved from Uniprot© database, allignment performed using Clustal Omega. All sequences have a reviewed status. The relative positions of ARL15, SAR1a and SAR1b are highlighted with a blue bar. Uniprot references of human: ARF1 (P84077); ARF3 (P61204); ARF4 (P18085); ARF5 (P84085); ARF6 (P62330); ARFRP (Q13795); ARL1 (P40616); ARL10 (Q8N8L6); ARL11 (Q969Q4); AR13A (Q5H913); AR13B (Q3SXY8); ARL14 (Q8N4G2); ARL15 (Q9NXU5); ARL16 (Q0P5N6); ARL17 (Q8IVW1); ARL2 (P36404); ARL3 (P36405); ARL4A (P40617); ARL4C (P56559); ARL4D (P49703); ARL5A (Q9Y689); ARL5B (Q96KC2); ARL5C (A6NH57); ARL6 (Q9H0F7); ARL8A (Q96BM9); ARL8B (Q9NVJ2); ARL9 (Q6T311); TRI23 (P36406); SAR1A (Q9NR31); SAR1B (Q9Y6B6).

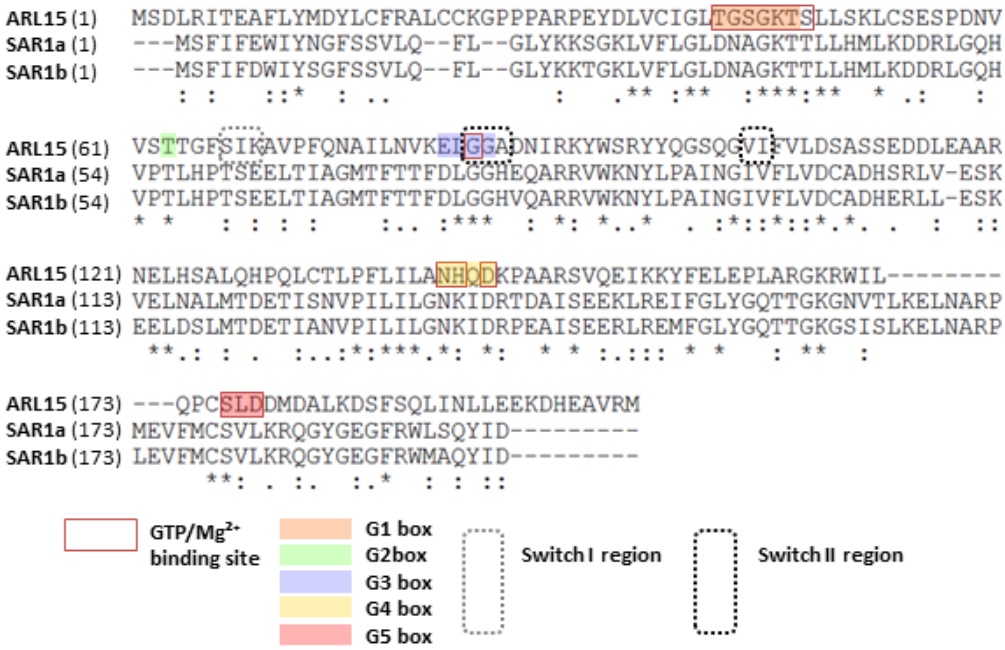

Figure S4. Alignment of human ARL15, SAR1a and SAR1b proteins. Sequences retrieved from Uniprot© database, alignment performed using Clustal Omega, with overall identity of 19%. Highlight of ARL15 predicted minor domains, associated with general catalytic functions of small GTPases; annotation retrieved from the NCBI© database. Sequence references: Q9NXU5, Q9NR31, Q9Y6B6.

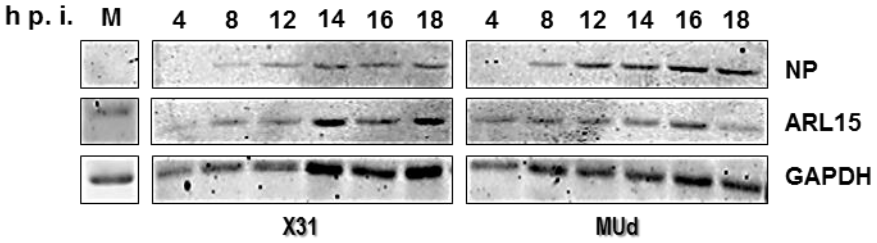

Figure S5. ARL15 levels during infection determined by western blot. A549 cells were infected at a MOI of 5 with IAV strains X31 and Mud, and harvested at 4, 8, 12, 14, 16 and 18h p.i.. Cell lysates were ran in a 15% acrylamide gel, transferred to a nitrocellulose membrane and stained for NP, ARL15 and GAPDH.

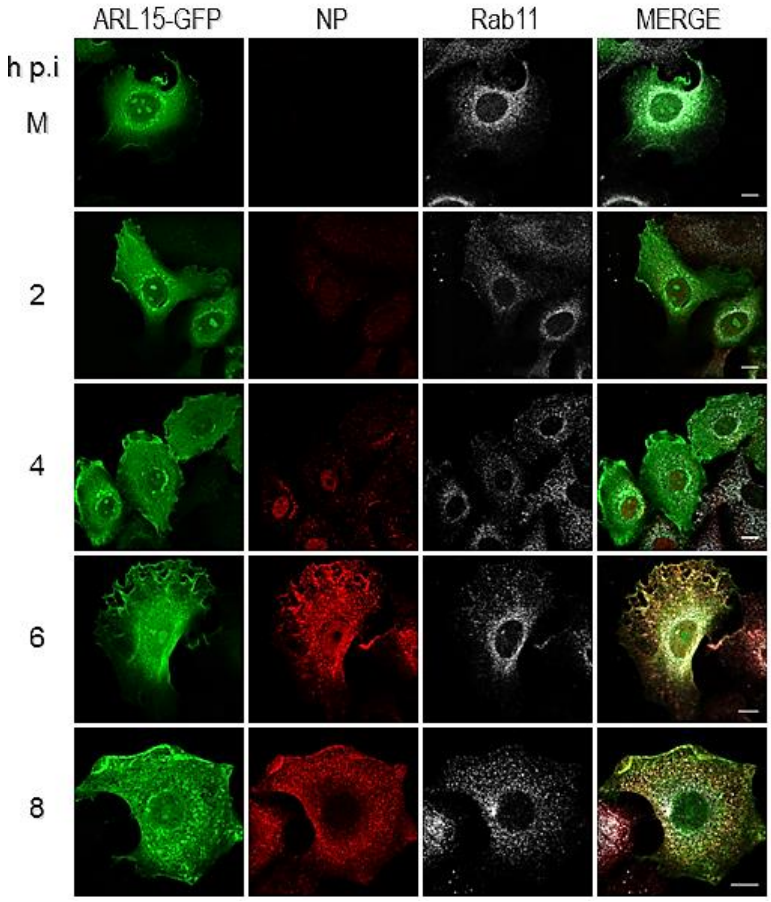

Figure S6. ARL15-GFP distribution during IAV infection. a) A549 ARL15-GFP stable cell lines were infected (MOI of 5). Cells were fixed in 4% PFA at 2h, 4h, 6h and 8h post-infection and stained against Rab11 and viral protein NP. Images acquired by confocal microscopy. Error bars of 10µm.

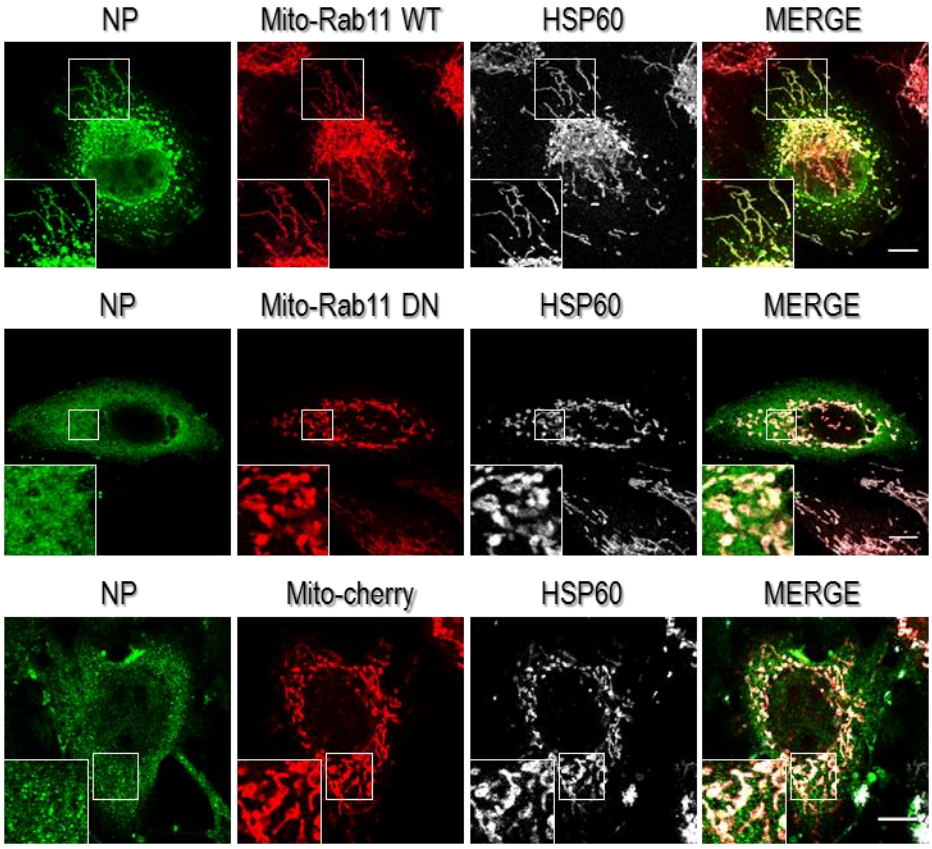

Figure S7. Mitochondria-targeted and cherry-tagged constructs. HeLa cells transfected with (top panel) pMitoRab11-WT (middle panel) pMitoRab11-DN and (bottom panel) pMito-cherry and infected (MOI of 20). Cells were fixed in 4% PFA 16h p.i. and stained against mitochondria protein HSP60 and viral protein NP. Images acquired by confocal microscopy. Error bars of 10µm.


U.PORTO
FACULDADE DE CIÊNCIAS
UNIVERSIDADE DO PORTO